cytoskeletal proteins, actin and tubulin, would exhibit cortical localization in ovulated oocytes. These two monoclonal antibodies (mAbs) are raised against the conserved domain of actin isoforms or β-tubulin. Confocal microscopic observation demonstrated that actin was asymmetrically localized in the oocyte: namely, metaphase II-arrested chromosomes enclosed by the actin were observed in one side of the oocyte cytoplasm (Supplementary Fig. S1b, c). In addition, actin was found to be concentrated on the cortical surface of the oocyte and appeared to exist as orderly arranged spots beneath the oocyte cell membrane (Supplementary Fig. S1d). Since tetraspanin CD9 is known to be present on the microvilli that regularly line the cell surface of an oocyte[8], oocytes were subjected to double staining with CD9 and actin mAbs. Neither protein was co-localized, and the actin-rich cortical area was clearly separated from the CD9-rich area (Supplementary Fig. S1d, e), implying the presence of at least two types of membranous structures in the oocyte cell membrane, as suggested previously[13]. Since CD9 plays an important role in sperm-oocyte fusion, but not sperm-oocyte adhesion[4], it was hypothesized that the actin-rich membranous structure on the cell surface of an oocyte may be involved in sperm-oocyte membrane 'adhesion'.

E-cadherin/β-catenin complex formation in both oocytes and sperm. Since E-cadherin/β-catenin complex has been known to bind to actin, by which cell-cell membrane adhesion is regulated[9], we considered that this E-cadherin/β-catenin complex may play a role as a regulator of sperm-oocyte membrane adhesion. To assess the problem, we first examined the possible interaction between E-cadherin/β-catenin complex and actin on an oocyte using immunocytochemical methods. In Fig. 1, subcellular localization of α- and β-catenins and E-cadherin is shown and data on the

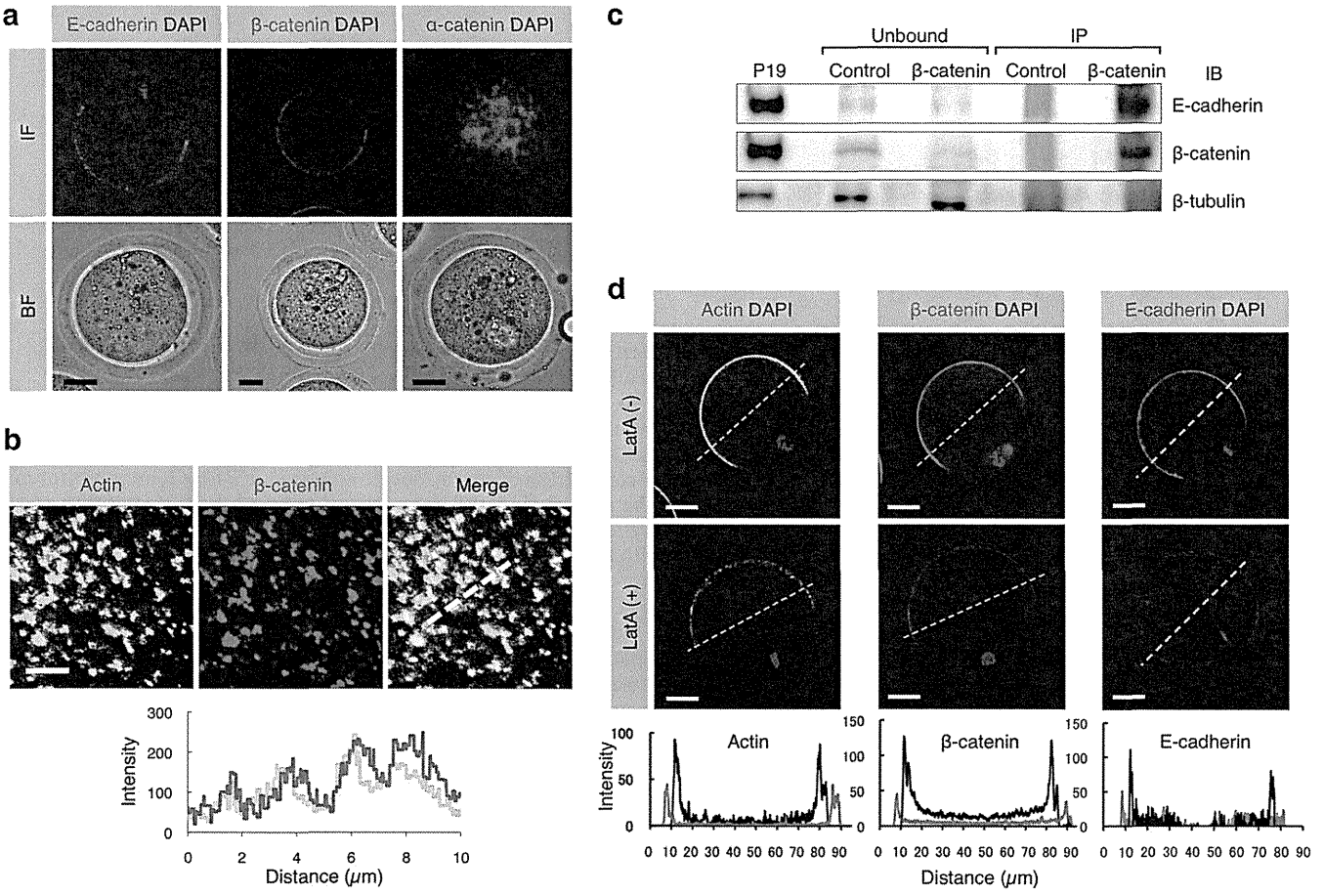

Figure 1 | Expression of E-cadherin and β-catenin and localization of E-cadherin/β-catenin complex in oocytes. (a) Localization of E-cadherin, β-catenin and α-catenin in ovulated oocytes. Similar distribution pattern of E-cadherin and β-catenin on an oocyte suggests complex formation between these two proteins. IF, immunofluorescence; BF, bright field. Scale bars: 20 μm. (b) Localization of β- and γ-actin isoforms and β-catenin beneath the oocyte cell membrane and their fluorescent intensities. The route scanned on the membrane was indicated as a dotted line. Fluorescence intensities for each protein were measured and graphed based on the 3D image, as described in the Experimental Procedures. Red and green lines in the lower panel indicate intensities of β-catenin and actin, respectively. Scale bar: 5 μm. (c) Biochemical evidence for the presence of E-cadherin/β-catenin complex in oocytes. The extract from 905 oocytes immunoprecipitated (IP) by anti-β-catenin mAb and mouse IgG purified from preimmune serum (Control) was subjected to immunoblotting with anti-E-cadherin, anti-β-catenin or anti-β-tubulin mAb. Extracts from mouse embryonic carcinoma cell line P19[35] were also subjected to immunoprecipitation with anti-β-catenin mAb and the resulting immunoprecipitates were reacted with each mAb as a positive control. Note that the extract (IP) immunoprecipitated by anti-anti-β-catenin mAb was reactive with both anti-β-catenin and anti-E-cadherin mAbs, but the extract (Unbound) that was not immunoprecipitated by anti-β-catenin mAb failed to bind to both antibodies. On the other hand, the β-tubulin was detectable in the Ab-unbound (but not Ab-IP) fractions. (d) Disassembly of β-catenin, E-cadherin and actin induced by latrunculin A (latA) treatment. Oocytes were doubly immunostained with anti-β- and γ-actin isoforms mAbs and DAPI (shown as 'Actin DAPI') or with anti-β-catenin mAb or with anti-E-cadherin mAb and DAPI (shown as 'β-catenin DAPI' or 'E-cadherin DAPI'). In the lower panels, the fluorescence intensities measured after being traced along dotted lines in the figures of the upper panels are shown. The intensities of latA-treated oocytes are indicated by red lines, while those of the latA-untreated oocytes are shown by black lines. Scale bar: 20 μm.

comparison between their localization and the localization of actin is also shown. Regarding the immunoreactivity of E-cadherin to an oocyte, a mAb that recognizes an N-terminal extracellular region of E-cadherin was used. Immunocytochemical staining demonstrated that E-cadherin was localized on the cell membrane (microvillar region) of an oocyte that has not been treated with permeabilization (Fig. 1a). β-catenin was detected beneath the oocyte cell membrane, and its localization pattern appeared to be similar to that of E-cadherin (Fig. 1a). In contrast, α-catenin was present in the oocyte cytoplasm (Fig. 1a). When the distribution of β-catenin on an oocyte was compared to that of actin, both proteins were found to be co-localized (Fig. 1b).

Secondly, we assessed the possible formation of β-catenin and E-cadherin complex using an immunoprecipitation method. A cell extract of mouse oocytes (n = 905) was immunoprecipitated with anti-E-cadherin mAb, and the resulting precipitate was then reacted with anti-β-catenin mAb. As a result, the cell extract immunoprecipitated with anti-E-cadherin mAb reacted with the anti-β-catenin mAb (Fig. 1c), indicating the presence of β-catenin and E-cadherin complex in an oocyte.

Thirdly, we assessed the effect of latrunculin A (latA), an inhibitor of actin polymerization, on the formation of β-catenin and E-cadherin complex. When oocytes were treated with 10 μM latA for 1 h at 37°C, actin immunoreactivity was reduced along with decreased immunoreactivity to β-catenin and E-cadherin (Fig. 1d). These results suggest that the β-catenin/E-cadherin complex formed in the oocyte cell membrane is closely associated with actin.

Since the β-catenin/E-cadherin complex is known to play a role in cell-cell adhesion via its homophilic interaction with E-cadherin[14], we predicted that this protein complex would also be produced in sperm. To test this hypothesis, epididymal capacitated sperm were collected from 10-week-old males and subjected to Western blotting (Fig. 2a) and immunoprecipitation (Fig. 2b) analyses. Western blotting revealed that both E-cadherin and β-catenin were detected in the sperm collected (Fig. 2a); however, N-cadherin was not detectable in those samples (Fig. 2a), although its expression has been reported in mouse oocytes[15]. Immunoprecipitation analysis also revealed the presence of the E-cadherin/β-catenin complex in sperm. The sperm extracts immunoprecipitated with anti-β-catenin mAb were reactive with anti-E-cadherin mAb, and those immunoprecipitated with anti-E-cadherin mAb were reactive with anti-β-catenin mAb (Fig. 2b). To confirm this further, immunocytochemical staining was performed for the isolated sperm. Staining of unpermeabilized sperm with anti-E-cadherin mAb demonstrated that E-cadherin was broadly expressed on the cell membrane of sperm from the head region to the mid-piece as well as part of the tail (Fig. 2c, d). Staining of permeabilized sperm with anti-β-catenin mAb revealed that the expression of β-catenin was localized beneath the sperm cell membrane and, notably, its localization pattern was similar to that of E-cadherin (Fig. 2c, d).

In mammals, both sperm-oocyte fusion and adhesion have been believed to occur in a specific region of the sperm head, called an equatorial segment (ES)[1]. Therefore, it is reasonable to consider that factor(s) regulating sperm-oocyte adhesion should exist in this segment. Since in the sperm head of the Asian musk shrew, *Suncus murinus*, ES is recessed within the waist of the sperm nucleus[16], it is easy to detect proteins localized in this segment. When immunocytochemical staining of the permeabilized shrew capacitated sperm was performed using anti-E-cadherin mAb, E-cadherin was expressed on the ES, the mid-piece and part of the tail (Supplementary Fig. S2a). Staining with anti-β-catenin mAb revealed the expression of β-catenin specifically localized on the ES of the sperm head (Supplementary Fig. S2b). Notably, its localization pattern was similar to that of E-cadherin in the shrew sperm (Supplementary Fig. S2a *vs.* Fig. S2b) and also to that of E-cadherin in the mouse sperm (Fig. 2c, d). Furthermore, some β-catenin molecules were released from the acrosomes of the shrew sperm (Supplementary Fig. S2b). Since the ES is recessed in the acrosome of the shrew sperm[16], β-catenin may have accumulated specifically in the ES upon completion of ES formation. These collected results led to a conclusion

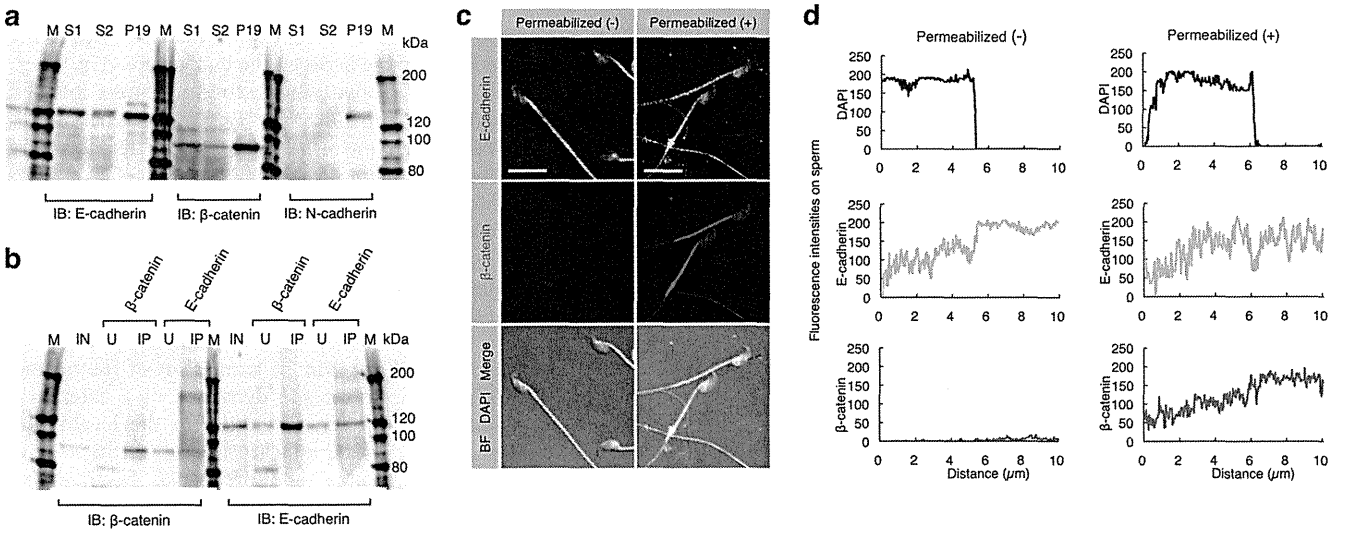

Figure 2 | Expression of E-cadherin and β-catenin and their interaction in sperm. (a) Expression of E-cadherin and β-catenin in epididymal sperm. E-cadherin and β-catenin, but not N-cadherin, in the sperm were detected by immunoblotting (IB). Sperm (S1 and S2) were collected from the epididymis of two males and used for IB. Extracts from P19 cells were used as a positive control. IB was performed using anti-E-cadherin, anti-β-catenin or anti-N-cadherin mAbs. M, molecular weight markers. (b) Interaction between E-cadherin and β-catenin in sperm. Extracts from the sperm (used as input sample (IN)) were immunoprecipitated by anti-E-cadherin or anti-β-catenin mAb. The precipitates (IP) and unbound extracts (U) were immunoblotted (IB) with anti-E-cadherin or anti-β-catenin mAb. M, molecular weight markers. (c) Localization of E-cadherin and β-catenin in sperm. Unpermeabilized or permeabilized sperm were doubly immunostained with anti-E-cadherin (ECCD-2) and anti-β-catenin mAbs, and their nuclei were stained with DAPI. ECCD-2, which recognizes an epitope in the N-terminal extracellular region of E-cadherin, bound to E-cadherin without permeabilization pretreatment. Scale bar: 5 μm. (d) The fluorescence intensity profiles of E-cadherin and β-catenin in sperm shown in (c). Fluorescence intensities were measured after being traced on the sperm along dotted lines shown at the bottom of the panels in (c).

that mammalian epididymal sperm always form E-cadherin/β-catenin complex.

Generation of *β-catenin*-, *α-catenin*- and *E-cadherin*-deficient oocytes. To determine which genes are involved in sperm-oocyte adhesion among *β-catenin*, *α-catenin* and *E-cadherin* genes, three strains (*E-cadherin*$^{floxed/floxed}$ [17], *β-catenin*$^{floxed/floxed}$ [18], and *α-catenin*$^{floxed/floxed}$ [19]) with *loxP*-flanked genes were inter-crossed with the transgenic mouse strain (*Tg*$^{ZP3\text{-}cre/+}$) expressing cre-recombinase in an oocyte-specific manner. Offspring (F2) lacking each type of gene (*E-cadherin*$^{floxed/floxed}$*Tg*$^{ZP3\text{-}cre/+}$, *β-catenin*$^{floxed/floxed}$*Tg*$^{ZP3\text{-}cre/+}$ and *α-catenin*$^{floxed/floxed}$*Tg*$^{ZP3\text{-}cre/+}$) were successfully obtained according to the Menderian inheritance rule (see Methods; Supplementary Fig. S3a), and were all viable and normal in size without displaying any overt physical or behavioral abnormalities. When the number of ovulated oocytes from these superovulated offspring was counted and compared with that of oocytes from the control floxed mice, there were no clear differences in the number of ovulated oocytes between the two groups: 11.7 ± 1.4 (n = 25) for *E-cadherin*$^{floxed/floxed}$*Tg*$^{ZP3\text{-}cre/+}$and 13.7 ± 1.9 (n = 22) for *E-cadherin*$^{floxed/floxed}$; 23.2 ± 1.5 (n = 21) for *β-catenin*$^{floxed/floxed}$*Tg*$^{ZP3\text{-}cre/+}$ and 23.2 ± 1.5 (n = 19) for *β-catenin*$^{floxed/floxed}$; 15.6 ± 2.4 (n = 9) for *α-catenin*$^{floxed/floxed}$*Tg*$^{ZP3\text{-}cre/+}$ and 12.4 ± 2.3 (n = 9) for *α-catenin*$^{floxed/floxed}$. Oocytes isolated from each line carrying the *cre-recombinase* gene were not morphologically distinguishable from those from each control floxed line (Supplementary Fig. S3b). To confirm whether oocytes from these gene-disrupted mice exhibit loss of target protein expression, oocytes were subjected to immunocytochemical staining together with oocytes from control floxed mice. E-cadherin, β-catenin and α-catenin were indeed absent from oocytes of *E-cadherin*$^{floxed/floxed}$*Tg*$^{ZP3\text{-}cre/+}$, *β-catenin*$^{floxed/floxed}$*Tg*$^{ZP3\text{-}cre/+}$ and *α-catenin*$^{floxed/floxed}$*Tg*$^{ZP3\text{-}cre/+}$, respectively (Supplementary Fig. S3b). These results suggest that these three genes are not essential for the maturation and ovulation of mouse oocytes.

In epithelial cells, β-catenin is required for localization of E-cadherin on the cell surface, and endocytosis of E-cadherin into the cytoplasm occurs in the absence of β-catenin[20]. In addition, a model was proposed: α-catenin participates to bind to the E-cadherin/β-catenin complex to connect with actin microfilaments under certain specific conditions[9]. In analogy to this, it is possible that cellular localization of E-cadherin, β-catenin and α-catenin is mutually regulated in oocytes. Such a possibility is already depicted in Fig. 1a, in which E-cadherin was co-localized with β-catenin, but not with α-catenin on a wild-type oocyte. To examine whether the formation of E-cadherin/β-catenin complex (possibly E-cadherin/β-catenin/α-catenin complex) is impaired when either one of these composite proteins is deficient, oocytes collected from all of the gene-ablated strains were immunocytochemically assessed for localization of these three proteins (Supplementary Fig. S4a–c). Expression of E-cadherin was strongly reduced on the cell membrane of *β-catenin*-deficient oocytes, but not *α-catenin*-deficient oocytes (Supplementary Fig. S4a *vs.* Fig. S4b). On the other hand, loss of E-cadherin did not affect the localization pattern of β-catenin and α-catenin (Supplementary Fig. S4c). Similar results were also obtained when *α-catenin*-deficient oocytes were examined (Supplementary Fig. S4a). These results indicate that β-catenin regulates the membrane localization of E-cadherin in mouse oocytes.

Sperm-oocyte adhesion or fusion assay. Membrane interaction between oocytes and sperm occurs after the penetration of sperm into ZP (Supplementary Fig. S1a). To monitor such interaction directly, 'ZP-free' *β-catenin*-deficient oocytes after enzymatic digestion of ZP were inseminated with wild-type epididymal sperm (Fig. 3a, b for adhesion assay; Fig. 3c–e for fusion assay). 'ZP-free' oocytes from *β-catenin*$^{floxed/floxed}$ mice were used as a control. When the oocytes were inspected 1 h after insemination and stained with 4',6-diamidino-2-phenylindole (DAPI) after fixation, as depicted in Fig. 3a, the number of sperm adhered to 'ZP-free' *β-catenin*-deficient oocytes was significantly reduced (Fig. 3b) compared to sperm bound to control oocytes. Similarly, when DAPI-preloaded oocytes were inspected 1 h after insemination, as depicted in Fig. 3c, the relative rate of 'ZP-free' *β-catenin*-deficient oocytes fused with sperm was also significantly reduced (39.2 ± 12.7 *vs.* 100.0 for control oocytes; $P<0.003$; Fig. 3d, e). We next examined the expression pattern of CD9, an essential protein for fusion[4], in *β-catenin*-deficient oocytes immunocytochemically and immunobiochemically to assess the ability of wild-type C57BL/6N sperm to fuse with their membrane. CD9 was expressed on the plasma membrane of 'ZP-free' *β-catenin*-deficient oocytes at a level comparable to that of 'ZP-free' control oocytes (Supplementary Fig. S5a). The total amount of CD9 quantified by immunoblotting in *β-catenin*-deficient oocytes was comparable to that of control oocytes (Supplementary Fig. S5b). These findings suggest that β-catenin is involved in sperm-oocyte adhesion.

***In vitro* fertilizing ability of *β-catenin*-deficient oocytes.** To know how fertilization is influenced by the dysfunction of sperm-oocyte adhesion, we determined the fertilization rate of *β-catenin*-deficient oocytes. The *β-catenin*-deficient oocytes surrounded by cumulus cells (herein referred to as 'cumulus-intact' oocytes) were isolated from oviducts and directly subjected to IVF with wild-type sperm, as depicted in Fig. 3f. 'Cumulus-intact' oocytes from *β-catenin*$^{floxed/floxed}$ mice were used as a control. When the oocytes were inspected 24 h after insemination, the relative rate of *β-catenin*-deficient oocytes fused with sperm was not reduced (Fig. 3g). Quantitative analysis revealed that the rate of *β-catenin*-deficient oocytes fused with sperm was rather enhanced (119.6 ± 4.6 *vs.* 100.0 for control oocytes; $P<0.02$; Fig. 3h), in contrast with the results of the previous adhesion/fusion assay (Fig. 3a–e). This is probably due to the occasional presence of the oocytes fused to sperm, which failed to develop to the two-cell stage; however, the fact that certain embryos developed to the two-cell stage would not exclude the possibility of pathogenetic activation of oocytes. On the other hand, the IVF rate (which is evaluated by the development of fertilized oocytes to the two-cell stage) was comparable between the two groups (Fig. 3i).

We further confirmed the above point by counting litters obtained through mating between *β-catenin*$^{floxed/floxed}$*Tg*$^{ZP3\text{-}cre/+}$ females and *β-catenin*$^{floxed/floxed}$ males. The control *β-catenin*$^{floxed/floxed}$ females were similarly mated. The litter size of *β-catenin*$^{floxed/floxed}$*Tg*$^{ZP3\text{-}cre/+}$ females was 5.3 ± 0.4, which was comparable with that of control females (5.8 ± 0.4) (Supplementary Fig. S6). These results indicate that oocytes lacking β-catenin expression reduce the ability to adhere with sperm, but sustain the ability to fuse with sperm as well as the total reproductive ability needed for delivering pups.

Possible involvement of β-catenin in transition of membrane adhesion to fusion. To examine the dynamics of β-catenin at sperm-oocyte membrane adhesion, alteration in the localization pattern of β-catenin at the sperm attachment sites of the *in vitro* fertilized "zona-free" oocyte was monitored (Fig. 4a–c). Before sperm attachment, β-catenin-rich patches (as shown in Fig. 1b) were clearly detected on the surface of an oocyte (upper left panel of Fig. 4a); however, these patches became undetectable 30 min after sperm attachment (arrows in the lower left panel; Fig. 4a). Furthermore, β-catenin was abundantly present in the capacitated sperm head (upper middle and right panels of Fig. 4a) before sperm attachment, but the amount of β-catenin in sperm heads was also greatly reduced after insemination (arrows in the lower middle and right panels; Fig. 4a). In addition, β-catenin was localized in the sperm head, although its localization pattern was slightly different in each sperm. Notably, β-catenin tended to be concentrated at ES (Fig. 2c; Supplementary Fig. S2; Fig. 4a).

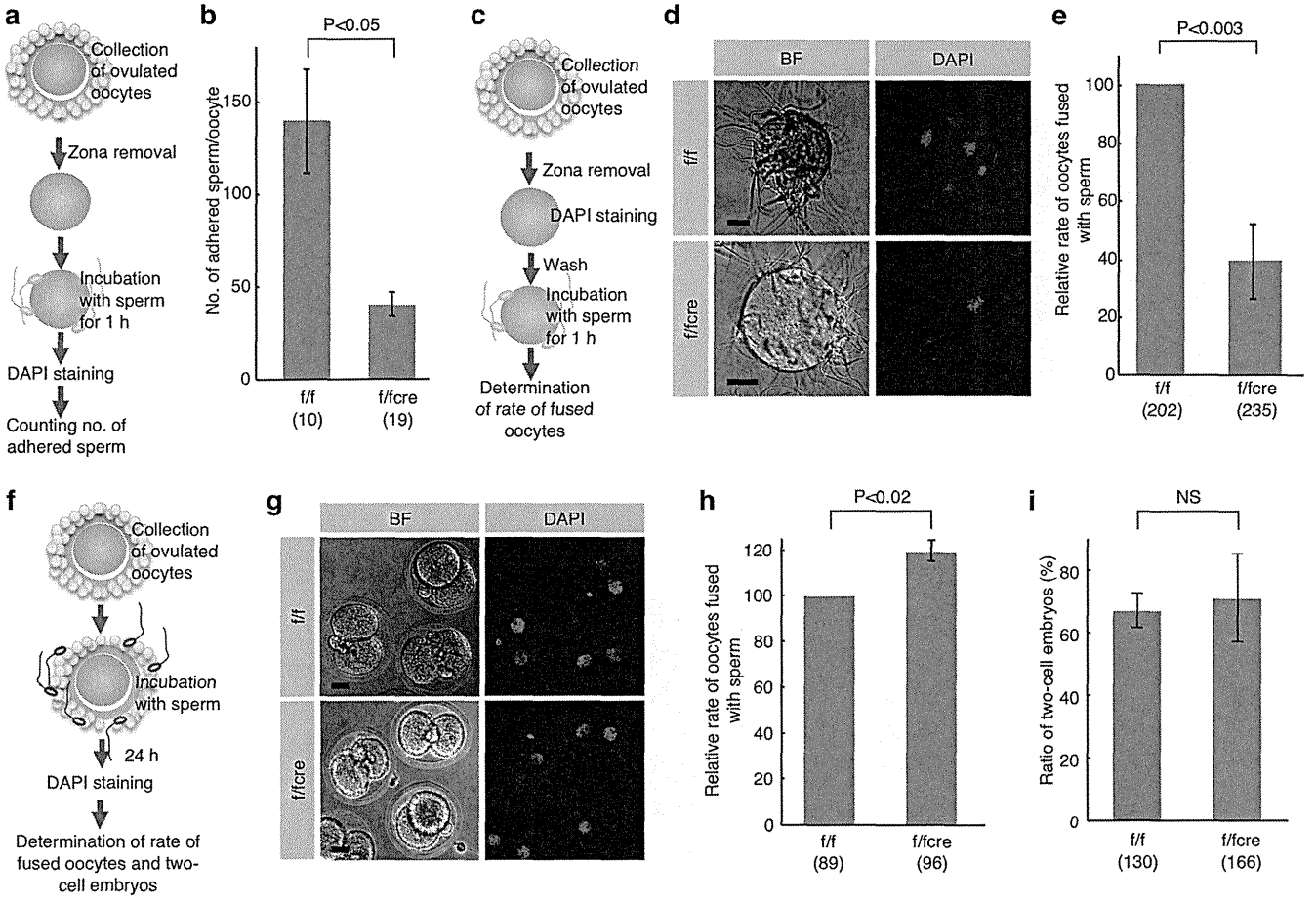

Figure 3 | *In vitro* fertilizing ability of *β-catenin*-deficient oocytes. (a) Experimental flow for testing sperm-oocyte membrane 'adhesion', and comparison of the number of wild-type sperm adhered to an 'zona-free' oocyte between f/fcre and f/f oocytes. After ZP removal, 'zona-free' oocytes were mixed with sperm for 1 h. (b) The number of sperm adhered to an oocyte was counted by DAPI-derived fluorescence in sperm heads on the surface of an oocyte. Parentheses indicate the number of oocytes examined. Values are the mean ± standard error (SE). (c) Experimental flow for testing sperm-oocyte membrane 'fusion' and fused sperm (shown as DAPI-positive sperm) in 'zona-free' *β-catenin*-deficient (f/fcre) and control (f/f) oocytes. After ZP removal, subsequent preincubation for 20 min in the presence of DAPI and washing, 'zona-free' oocytes were mixed with the wild-type sperm for 1 h. (d) Comparison of oocytes fused with sperm between f/fcre and f/f oocytes. BF, bright field. Bars: 20 μm. (e) Comparison of the relative rate of oocytes fused with sperm between f/fcre and f/f oocytes. Only oocytes having at least one fused sperm were counted. The comparative values relative to the control (f/f oocytes; set to 100.0) were displayed as the relative rate of fused oocytes. Parentheses indicate the number of oocytes examined in triplicate experiments. Values are the mean ± SE. (f) Experimental flow for testing sperm-oocyte membrane interaction and fused sperm in two-cell embryos developing from 'cumulus-intact' *β-catenin*-deficient (f/fcre) and control (f/f) oocytes. DAPI staining was performed to detect fused sperm on the developing two-cell embryos. (g) Comparison of oocytes fused with sperm between "cumulus-intact" f/fcre and f/f oocytes. Bars: 20 μm. (h) Comparison of the relative rate of oocytes fused with sperm between "cumulus-intact" f/fcre and f/f oocytes. Parentheses indicate the number of oocytes examined in triplicate experiments. Values are the mean ± SE. (i) Comparison of the ratio of oocytes developing to two-cell stage 24 h after fertilization between "cumulus-intact" f/fcre and f/f oocytes, according to the procedure described in (f). Parentheses indicate the total number of oocytes examined in triplicate experiments. NS, not significant. Values are the mean ± SE.

These findings could also be supported by measurement of fluorescent intensities of β-catenin (Fig. 4b, c). When fluorescence intensity at the equator of an oocyte (dotted line in the upper image of the left panels; Fig. 4a) was compared with that in the region of an oocyte adhered to sperm (dotted line in the lower image of the left panels; Fig. 4a), intense localization of β-catenin in the oocyte exhibiting no sperm attachment was observed beneath the oocyte membrane (arrows in the upper graph; Fig. 4b); however, 30 min after sperm attachment, the fluorescent intensity of β-catenin beneath the oocyte membrane was markedly reduced (arrows in the lower graph; Fig. 4b). Concomitantly, fluorescence intensity throughout the entire sperm (dotted lines in the right panels; Fig. 4a) was quantitatively compared before and after sperm adhesion to the oocyte membrane (Fig. 4c). Before attachment to the oocyte membrane, β-catenin was broadly localized in the sperm head (corresponding to the DAPI-stained region), mid-piece and part of the tail (Fig. 2c, d; upper graph of Fig. 4c); however, after attachment to the oocyte membrane, the intensity of β-catenin in the sperm head (but not in a mid-piece and tail) was markedly decreased (arrows in the lower middle and right panels of Fig. 4a; lower graph of Fig. 4c). Moreover, to confirm that the amount of β-catenin is reduced at steps between sperm-oocyte adhesion and fusion, localization pattern of β-catenin at the sperm attachment sites of the *in vitro* fertilized "zona-free" *CD9*-deficient oocyte was monitored (Fig. 4d, e). Before sperm attachment, intense localization of β-catenin (as shown in the upper left panel of Fig. 4a) was clearly seen on the surface of an oocyte (upper middle panel of Fig. 4d); however, these patches became undetectable 30 min after sperm attachment (arrows in the lower middle panel; Fig. 4d). These findings were also confirmed by measurement of fluorescent intensities of β-catenin (Fig. 4e). When

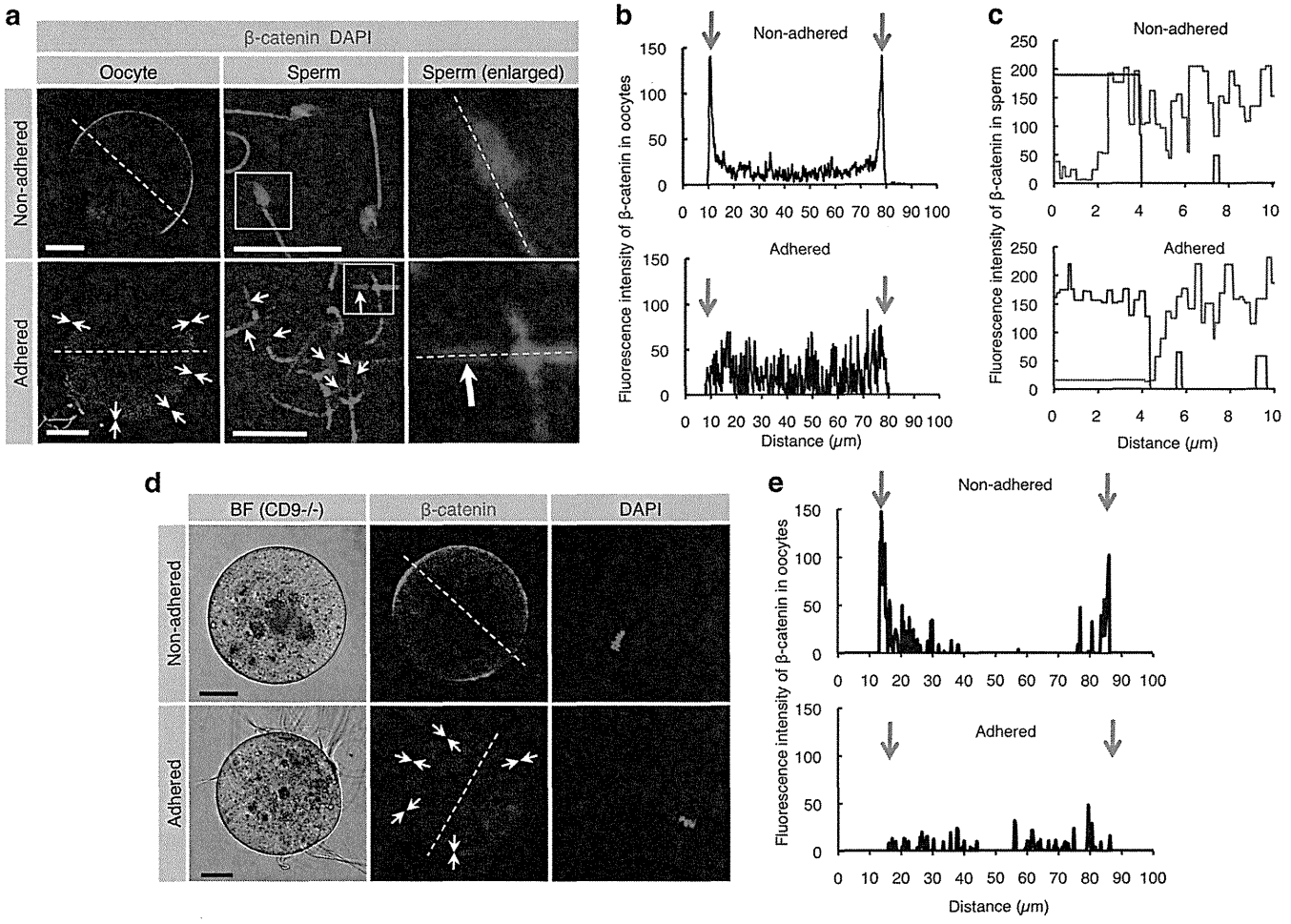

Figure 4 | Reduced levels of β-catenin localized beneath the cell membrane of both oocytes and sperm after membrane adhesion. (a) β-catenin disassembly induced by membrane adhesion in oocytes and sperm. In the 'Non-adhered' group (upper panels), ZP-denuded C57BL/6N oocytes were stained with DAPI and subsequently reacted with anti-β-catenin mAb. Also, epididymal sperm were stained with DAPI and anti-β-catenin mAb. In the 'Adhered' group (lower panels), ZP-denuded C57BL/6N oocytes were stained with DAPI and then subjected to IVF for 30 min prior to incubation with anti-β-catenin mAb. Arrows indicate areas where fluorescent intensities of β-catenin are reduced. In each panel, boxes in middle sets of panels were enlarged and shown on the right. Scale bars: 20 and 10 μm in left and middle panels, respectively. (b) Fluorescence intensities of oocytes before and after sperm-oocyte adhesion. Fluorescence intensities were measured after being traced along dotted lines in the left panels of (a). Arrows indicate both sides of the oocyte cell membranes. (c) Fluorescence intensities of sperm before and after sperm-oocyte adhesion. Fluorescence intensities were measured after being traced along dotted lines in the right panels of a. Red and blue lines indicate fluorescent intensities for β-catenin and DAPI, respectively. (d) β-Catenin disassembly induced by membrane adhesion in oocytes and sperm. In the 'Non-adhered' group (upper panels), ZP-denuded *CD9-/-* oocytes were stained with DAPI and subsequently reacted with anti-β-catenin mAb. In the 'Adhered' group (lower panels), ZP-denuded *CD9-/-* oocytes were preloaded with DAPI as depicted in Fig. 3c and then subjected to IVF for 30 min prior to incubation with anti-β-catenin mAb. Arrows indicate areas where fluorescent intensities of β-catenin are reduced. In each panel, Scale bars: 20 μm. (e) Fluorescence intensities of *CD9-/-* oocytes before and after sperm-oocyte adhesion. Fluorescence intensities were measured after being traced along dotted lines in the left panels of d. Arrows indicate both sides of the oocyte cell membranes.

fluorescence intensity at the equator of an oocyte (dotted line in the upper image of the middle panel; Fig. 4d) was compared with that in the region of an oocyte adhered to sperm (dotted line in the lower image of the middle panel; Fig. 4d), intense localization of β-catenin in the oocyte exhibiting no sperm attachment was observed beneath the oocyte membrane (arrows in the upper graph; Fig. 4e); however, 30 min after sperm attachment, the fluorescent intensity of β-catenin beneath the oocyte membrane was markedly reduced (arrows in the lower graph; Fig. 4e). These collective data imply that alteration in the localization of β-catenin in both sperm and oocyte membranes may contribute to the transition of cell adhesion to fusion.

Generally, in the absence of Wnt signal, E-cadherin-free cytoplasmic β-catenin is rapidly degraded due to "ubiquitination", while only membrane-anchored β-catenin, which is associated with E-cadherin, is resistant to such degradation[21]. Since the fluorescence intensity of β-catenin beneath cell membranes was greatly reduced in both sperm and oocytes after membrane adhesion, ubiquitination may be involved in such reduction. In other words, degradation of β-catenin may be involved in the transition from adhesion to fusion upon sperm-oocyte interaction. To test this possibility, we employed an inhibitor of the ubiquitination pathway to investigate whether it can disturb sperm-oocyte fusion. UBE1-41, a specific inhibitor of ubiquitin-activating enzyme 1 (UBE1), is known to impair antigen-induced FcεRI ubiquitination and internalization[22] and to inhibit melanocortin-4 receptor internalization via ubiquitination[23]. To determine the optimal concentration of UBE1-41, we first assessed sperm-oocyte interaction by co-incubation of sperm and

oocytes in TYH medium containing various amounts of UBE1-41 (0, 1, 5, 10, 20 or 50 μM). We finally decided to use 10 μM UBE1-41, because treatment with more than 20 μM UBE1-41 caused deleterious effects on oocytes. Notably, this concentration (10 μM) appears to be lower than that (50 μM) reported previously[22]. "Zona-free" oocytes treated with 10 μM UBE1-41 for 30 min were incubated with sperm and the ratio of fused oocytes was measured (Fig. 5a). As depicted in Fig. 4a, c, the fluorescence intensity of β-catenin beneath cell membranes was greatly reduced in the untreated oocyte after membrane adhesion with sperm (arrows in the upper left panel; Fig. 5b); however, intense localization of β-catenin was observed beneath the oocyte membrane in the oocyte treated with UBE1-41 even after membrane adhesion with sperm (arrows in the lower left panel; Fig. 5b), and β-catenin-rich patches (oocyte before membrane adhesion; Fig. 1b) were clearly detected on the surface of the oocyte (lower right panel; Fig. 5b). The rate of oocyte fusion with sperm was inversely correlated with the intense localization of β-catenin beneath the cell membrane: treatment with UBE1-41 lowered the rate of fused oocytes in contrast with that of untreated oocytes (51.7 ± 6.2 for UBE1-41-treated oocytes *vs.* 100.0 for untreated oocytes; $P<0.0001$; Fig. 5c; Supplementary Fig. S7). This result suggests that β-catenin ubiquitination leading to degradation is involved in transition from membrane adhesion to fusion. Given this background, it seems likely that the loss of β-catenin facilitates sperm-oocyte fusion. In other words, the fusing ability of *β-catenin*-deficient oocytes should be unaffected by treatment with UBE1-41. In fact, *β-catenin*-deficient oocytes exhibited fusing ability, although they were unable to adhere to sperm (Fig. 3). Furthermore, treatment of $\beta\text{-catenin}^{floxed/floxed}Tg^{ZP3\text{-}cre/+}$ oocytes with UBE1-41 did not affect the rate of fused oocytes (90.6 ± 11.3 for UBE1-4-treated oocytes *vs.* 100.0 for untreated oocytes; Fig. 5d). By contrast, similar treatment of $\beta\text{-catenin}^{floxed/floxed}$ oocytes resulted in reduction of their fusing ability, as expected (55.3 ± 11.5 for UBE1-4-treated oocytes *vs.* 100.0 for untreated oocytes; $P<0.02$; Fig. 5d). These results led us

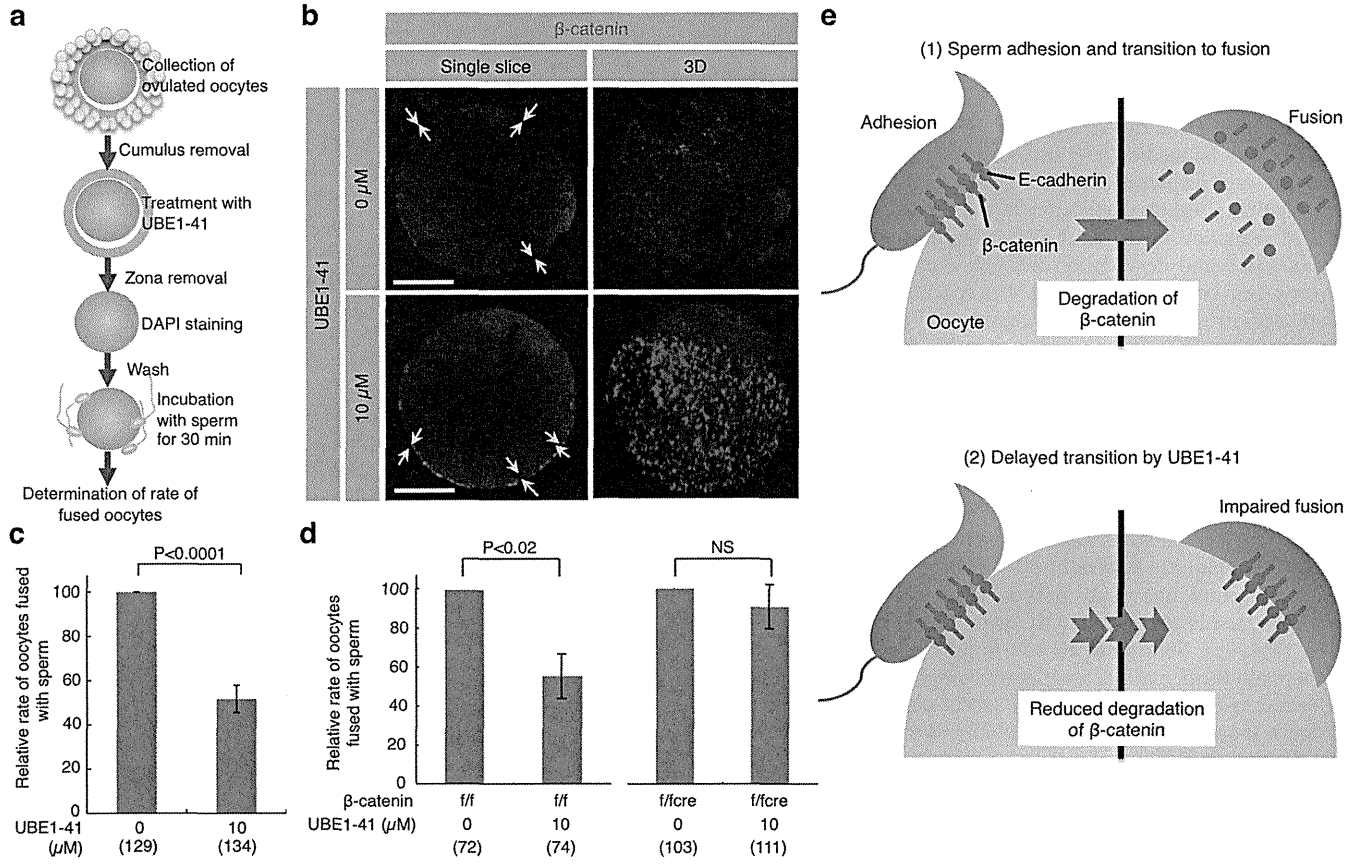

Figure 5 | Reduced fusing ability of oocytes treated with UBE1-41, an inhibitor of ubiquitination. (a) Experimental flow. Cumulus cells attached to the oocytes collected from oviducts were removed. The oocytes were then treated with UBE1-41 for 30 min, followed by ZP removal. After 20-min incubation with DAPI-containing medium and subsequent washing, 'zona-free' oocytes were mixed with the sperm and incubated for 30 min. Only oocytes having at least one fused sperm were counted as fused oocytes. (b) Sustained expression of β-catenin on the surface of "zona-free" wild-type oocytes treated with UBE1-41 after membrane adhesion with sperm. Arrows indicate oocyte cell membranes where β-catenin deposition is noted. One sperm fused with the untreated oocyte (upper panel), but not with the UBE1-41-treated oocyte (lower panel). To focus on the β-catenin expression, only fluorescent images are shown. Single slice, Image captured when the diameter of an oocyte was longest; 3D, 3-dimensional image reconstructed from serial scanned images. Bars: 20 μm. (c) Decreased number of fused sperm on "zona-free" wild-type oocytes after treatment with UBE1-41. The relative rate of oocytes carrying fused sperm was compared between UBE1-41-treated and -untreated wild-type oocytes. The comparative values relative to the control (set to 100.0) are displayed as the relative rate of fused oocytes. As described in the legend of Fig. 3c, oocytes fused with sperm are defined as those with at least one DAPI-positive sperm. (d) Comparison of the relative rate of oocytes carrying fused sperm between UBE1-41-treated and untreated oocytes (*β-catenin*-deficient (f/fcre) *vs. β-catenin*-intact (f/f) oocytes). Comparison was made as described in (c). NS, not significant. Parentheses indicate the total number of oocytes examined in triplicate experiments. Values are the mean ± SE. (e) A model of the possible role of β-catenin in transition from membrane adhesion to fusion. At fertilization (as described in (1)), adhesion of sperm to the surface of an oocyte is mediated by E-cadherin/β-catenin complex; however, subsequent fusion requires rapid degradation of β-catenin. On the other hand, in the presence of UBE1-41 (as described in (2)), adhesion occurs normally, but fusion is impaired since UBE1-41 inhibits degradation of β-catenin.

to consider that β-catenin may be accumulated around sperm attachment sites through the formation of a protein complex with E-cadherin, but immediately diminished when sperm-oocyte fusion occurred. This transient formation of such complex encouraged us to suppose that the E-cadherin/β-catenin complex plays an important role in the transition from membrane adhesion to membrane fusion during sperm-oocyte interaction (Fig. 5e).

Discussion

Membrane fusion occurs after membrane adhesion. Such a process is also true for sperm-oocyte interaction[1]. Our present results indicate that both E-cadherin and β-catenin are involved in sperm-oocyte membrane adhesion. This is demonstrated by the fact that *β-catenin*-deficient oocytes can fuse to sperm, and develop normally to term.

E-cadherin is involved in homophilic adhesion between epithelial cells, and transduces external signaling via α-catenin and β-catenin[9]. In contrast, E-cadherin remains essential for basic cell-cell adhesion, even in the absence of α-catenin, in human prostate carcinoma PC3 cells[24], suggesting that the formation of E-cadherin/β-catenin/actin microfilament complex is proceeded by other molecule(s) in the absence of α-catenin. In analogy, at sperm-oocyte adhesion, association between the E-cadherin/β-catenin complex and actin microfilaments may be mediated by molecule(s) other than α-catenin or the E-cadherin/β-catenin complex itself can directly bind to actin microfilaments, although evidence for this remains to be provided.

Rapid reduction in the level of β-catenin occurs after increased ubiquitination and degradation through a proteosomal pathway[21]. N-Acetyl-Leu-Leu-Nle-CHO (ALLN), a specific inhibitor of the proteolytic activity of proteasomes is reported to inhibit sperm-oocyte fusion upon fertilization[25], implying that the ubiquitination-proteasome pathway may play a role in sperm-oocyte interaction by regulating the quantity of β-catenin on sperm and oocyte membranes. Giving that β-catenin is present on the sperm head and oocyte surface, and that its elimination impairs sperm-oocyte adhesion (see Fig. 3b), it is conceivable that the ubiquitination-proteasome pathway is a key that mediates phase transition from membrane adhesion to fusion, as genetic studies in *C. elegans* have identified multiple roles for the ubiquitin system in early development[26].

Taken together, our results propose a model regarding the transition from membrane adhesion to fusion upon sperm-oocyte interaction (Fig. 5e). Before sperm-oocyte adhesion, both sperm and oocyte retain the β-catenin/E-cadherin complex, a complex important for sperm-oocyte adhesion. Once sperm-oocyte adhesion occurs, β-catenin is immediately ubiquitinated and probably degraded in both the sperm and oocyte, thereby initiating membrane fusion between these two cells; however, in oocytes treated with UBE1-41, ubiquitination of β-catenin associated with sperm-oocyte adhesion is suppressed, which will cause impaired fusion between sperm and oocyte. This sperm-oocyte adhesion and subsequent fusion appears to be each independent phenomena, since the absence of β-catenin results in a reduction in the ability of sperm to adhere to an oocyte, but sperm-oocyte membrane fusion occurs normally.

Similarly, importance of interchange between stabilization and degradation of β-catenin has been described at several developmental aspects, such as mesenchymal cell proliferation[27] and primordial germ cell development[28]. Forced expression of a mutated β-catenin that is resistant to degradation causes developmental arrest at specific sites and time[27,28]. However, its deficiency has no impact on embryogenesis, probably due to compensation of other molecules that play roles similar to β-catenin[27, 28]. Probably, degradation of β-catenin that occurs at appropriate stage and place is needed for normal development of an embryo/fetus and therefore β-catenin may be an important molecule that mediates as a molecular switch in embryogenesis. Our present results showed that although the cell membrane of *β-catenin*-deficient oocytes exhibit reduced ability to adhere sperm (Fig. 3b), these oocytes could be successfully fertilized, indicating that β-catenin contributes partly to sperm-oocyte membrane adhesion, but does not play an essential role in this event. It will be claimed that ZP removal by acidic Tyrode's solution can change cell surface protein composition or carbohydrate structure, which may affect sperm-oocyte interaction to some extents. Our present data, however, clearly suggest that β-catenin degradation is associated with transition from adhesion to fusion upon interaction between sperm and oocyte.

In human trophoblastic cells, an interrelationship between cell differentiation/ fusion and reduced expression of E-cadherin has been pointed out[29]. When the isolated mononuclear cytotrophoblasts are cultured, they tend to aggregate and then fuse to form syncytia. During this process, E-cadherin is detectable at the cell-cell contact sites of an aggregate. However, the fusing cytotrophoblasts (but not non-fusing cytotrophoblasts) exhibit marked reduction in the level of E-cadherin. Notably, exposure of the non-fusing cells to 8-bromo cyclic AMP causes reduced expression of E-cadherin, and induces their cellular fusion and syncytium formation. These results suggest that down-regulation of E-cadherin gene expression coincides with cell fusion, and evoke us to suppose that remodeling of the adhesion complex on the cell surface would induce subsequent cell fusion. Beside E-cadherin, junctional proteins found in tight and adherens junctions such as integral membrane, adaptor, regulator and signaling proteins are recently thought to be important as epithelial and endothelial barriers[30]. They can reversibly increase paracellular transport and drug delivery with less toxicity, indicating that alteration in lipid composition at cell surface membrane, as exemplified by alteration of cholesterol efflux, results in modulation of cellular junctions. Based on these results, we consider that remodeling or degradation of adhesion complex may change lipid composition in a cell membrane, which will then provide microenvironments where cell fusion occurs.

When the fusion step is genetically defective, sperm never fuses with the partner oocyte, as previously shown by using *CD9*-deficient oocytes and *Izumo1*-deficient sperm[3,5,6]. Furthermore, we showed that the presence or absence of β-catenin in oocytes does not affect the expression and localization of CD9 (see Supplementary Fig. S5). In addition, we also observed that the presence or absence of CD9 does not affect the change of β-catenin localization in oocytes before and after adhesion to sperm (see Fig. 4d, e). A couple of these results suggest that β-catenin is independent from CD9 tetraspanin network. These findings evoked us to suppose that the adhesion step may be distinguishable from the fusion step in mammalian fertilization. Interestingly, Jégou *et al.* (2011) recently demonstrated that CD9 is indeed involved in the sperm-egg binding step. This suggests a possible role of CD9 in sperm-oocyte adhesion, but does not exclude the previous finding that CD9 is involved in fusion[31]. Although further investigation on the role of CD9 molecule in sperm-oocyte adhesion and subsequent fusion is needed, it seems likely at present that CD9 may be involved in maintaining the strength of adhesion force on the oocyte cell membrane. Its absence would cause unstable adhesion force, resulting in decreased fertilizing ability of sperm.

In conclusion, we have shown that 1) β-catenin plays a role in sperm-oocyte membrane adhesion upon fertilization; and 2) β-catenin is also involved in the transition of membrane adhesion to fusion, a phenomenon essential for fertilization, and proteasome-mediated regulation of β-catenin is important in such sperm-oocyte fusion.

Methods

Antibodies. Two mAbs against mouse E-cadherin used for immunostaining and immunoblotting (No. ECCD-2; Takara-Bio) and immunoprecipitation (No. 36; BD). Two mAbs against mouse β-catenin were used for immunoprecipitation (No. C2206; Sigma) and immunostaining (No. 15B8; Sigma). A mAb against β-catenin (No. 14; BD) was used for immunoblotting. A polyclonal antibody against mouse α-catenin

(No. C2081; Sigma), Cy3-conjugated mAb against C-terminal peptide conserved in β- and γ-actin isoforms (No. AC-40; Sigma), and FITC-conjugated mAb against β-tubulin (No. TUB2.1; Sigma) were used. A mAb against N-cadherin was used for immunoblotting (No. 32; BD). ECCD-2, which recognizes an epitope in the extracellular region of E-cadherin, bind to E-cadherin on the cell membrane without permeabilization[32].

Immunostaining. Mouse oocytes were collected from oviducts of 8- to 12-week-old C57BL/6N superovulated mice (Japan SLC Inc.). The oocytes were fixed for 20 min at room temperature in a solution (termed PFA-GLA-PVP) containing 2% paraformaldehyde (PFA), 0.1% glutaraldehyde (GLA) and 0.1% polyvinylpyrolidone (PVP). After washing in phosphate-buffered saline (PBS), they were permeabilized with 1% Triton X-100 in PBS, and washed 3 times in PBS. The oocytes were then incubated with the primary antibodies (Abs) (2.5 μg/ml) in HEPES-buffered saline (HBS) containing 10 mM HEPES (pH 8.0), 0.15 M NaCl and 3% fetal bovine serum (FBS) for 2 h at 4°C. These oocytes were next treated with the secondary Abs (1.25 μg/ml), Alexa488- or Alexa546-conjugated IgG (Molecular Probes), and washed 3 times in HBS. Mouse sperm were also isolated from the cauda epididymides of 8- to 12-week-old C57BL/6N male mice by teasing them in TYH medium[33], and immunostained as described above. In addition, sperm were collected from 24-week-old KAT strain[16] males of the *Suncus murinus*, kindly provided by Dr. Senichi Oda and immunostained as described above. These immunostained sperm were then counterstained with DAPI (WAKO) at the final concentration of 10 μg/ml in HBS for 30 min at 4°C, and washed 3 times by transfer to HBS.

Sectioned fluorescent images were captured by a confocal microscope (LSM 510 model; Carl Zeiss), and transformed into three-dimensional (3D) images by LSM Image Brower Version 4.2.0.121. The fluorescence intensities of target proteins were then measured based on the 3D images (Supplementary Fig. S1d, e; Fig. 1b), and compared between latA-untreated and -treated oocytes (Fig. 1d), unpermeabilized and permeabilized sperm (Fig. 2c, d), and oocytes and sperm before and after membrane adhesion (Fig. 4a–c). All animal experiments were performed according to protocols approved by the Institutional Animal Care and Use Committee at the National Institute for Child Health and Development.

Immunoblotting and immunoprecipitation. The sperm suspension (ca. 3.0×10^6 cells) prepared from C57BL/6N males was collected by centrifugation, as described by Inoue *et al.*[3] A total of 200 oocytes were collected and then lysed in Laemmli's SDS sample buffer, boiled, resolved in SDS-PAGE on an 8% acrylamide gel, and immunoblotted as described previously[34]. Mouse embryonic carcinoma P19 cells[35] were were used as a positive control. For immunoprecipitation, Sakakibara *et al.*[34] describe this procedure in more detail citing references[36]. Proteins from sperm (ca. 3.0×10^6 cells) (Fig. 2b) or 905 oocytes (Fig. 1c) were immunoprecipitated with Abs (2.5 μg/ml) for 6 h at 4°C. The presence of β-tubulin was detected and used as an internal loading control.

Actin disassembly induced by latA treatment. Mouse oocytes collected from oviducts of superovulated mice were incubated in TYH medium containing 10 μM latA (Molecular Probes) for 1 h at 37°C, and fixed in PFA-GLA-PVP solution. After permeabilization with 1% Triton X-100, oocytes were doubly immunostained by mAbs against actin and β-catenin as mentioned in the 'Immunostaining' section. The fluorescence intensities at the equator, as indicated by dotted lines, were then analyzed as described in the 'Immunostaining' section.

Generation of mice with gene-ablated oocytes. To produce oocytes with a single gene deleted, floxed mutant mice for *E-cadherin*[17], *β-catenin*[18] or *α-catenin* gene[19] were cross-mated with transgenic (Tg) mice expressing *cre-recombinase* in an oocyte-specific manner under the control of oocyte-specific ZP protein 3 (ZP3) promoter ($Tg^{ZP3\text{-}cre/+}$), kindly provided by Dr. Barbara B. Knowles[37]. The F1 offspring, so-called *E-cadherin*$^{floxed/floxed}Tg^{ZP3\text{-}cre/+}$, *β-catenin*$^{floxed/floxed}Tg^{ZP3\text{-}cre/+}$ and *α-catenin*$^{floxed/floxed}Tg^{ZP3\text{-}cre/+}$, were propagated through brother-sister mating. The presence of the *cre-recombinase* gene in these offspring was detected by PCR analysis using the following set of primers: Cre-S (5'-TGATGAGGTTCGCAAGAACC-3'; nucleotide no. 170 to 189 (GenBank Accession no. AB449974.1)) and Cre-A (5'-CCATGAGTGAACGAACCTGG-3'; nucleotide no. 539 to 558 (GenBank Accession no. AB449974.1)); this primer set yielded a band of 389 bp.

Determination of litter size and *in vitro* fertilization (IVF). To determine the litter size, the number of pups delivered from an 8- to 12-week-old female (offspring of *β-catenin*$^{floxed/floxed}Tg^{ZP3\text{-}cre/+}$ mice) was recorded after mating for two months by placing an 8- to 12-week-old C57BL/6N male in the cage.

For IVF, oocytes were collected from the oviductal ampulla region of superovulated *β-catenin*$^{floxed/floxed}Tg^{ZP3\text{-}cre/+}$ females (8 to 12 weeks old) 14 to 16 h after hCG injection, and placed in a 30-μl drop of TYH medium covered with paraffin oil (Nacalai) equilibrated with 5% CO_2 in air at 37°C. Sperm collected from the epididymides of 8- to 12-week-old C57BL/6N males were induced to capacitate by incubating in TYH medium for 90 min in an atmosphere of 5% CO_2 in air at 37°C before insemination. The final concentration of sperm added to the oocytes was 1.5×10^5 sperm/ml. The oocytes collected from *floxed/floxed* mice were also inseminated with C57BL/6N sperm as a control.

To count the number of sperm fused to an oocyte, cumulus cells were dispersed from oocytes by incubating them for 10 min at 37°C in TYH medium containing hyaluronidase (300 μg/ml; Merk4Biosciences), and then the oocytes were denuded of the ZP by brief incubation in acid Tyrode's solution (Sigma). The 'zona-free' oocytes were preincubated with DAPI at the final concentration of 10 μg/ml in TYH medium for 20 min at 37°C, and washed 3 times by being transferred to separate drops of TYH medium. DAPI is a fluorescent dye that can slowly permeate the living cell membrane (semi-permeable) and hardly leaks out of cells after washing, relative to Hoechst33342 (permeable), as shown in Invitrogen's instructions. This preincubation procedure with DAPI enables the staining of only fused sperm nuclei, probably through a mechanism in which the dye present within an oocyte is transferred to fused sperm upon membranous fusion. C57BL/6N sperm (ca. 1.5×10^5 sperm/ml) were added to a 30-μl drop of TYH medium containing 30 DAPI-treated 'zona-free' oocytes and then the dish was incubated for 1 h at 37°C. After incubation, the oocytes were fixed with PFA-GLA-PVP solution for 20 min at room temperature. The rate of oocytes fused with sperm was determined by counting DAPI-transferred sperm on an oocyte under a fluorescence microscope. In this case, oocytes fused with sperm were defined as those with at least one DAPI-positive sperm. Moreover, in a separate group in which 'zona-intact' oocytes were incubated with sperm for 24 h at 37°C and then stained by DAPI, the rate of those oocytes to develop to the two-cell stage was determined under a stereoscopic microscope without fixation.

To count the number of sperm adhered to an oocyte, cumulus cells were dispersed from oocytes in TYH medium containing hyaluronidase (Merk4Biosciences), and the oocytes were denuded of the ZP by incubation in acid Tyrode's solution (Sigma). The C57BL/6N sperm (ca. 1.5×10^5 sperm/ml) were added to a 30-μl drop of TYH medium containing 30 'zona-free' oocytes and then the dish was incubated for 1 h at 37°C. After incubation, the oocytes were fixed with a PFA-GLA-PVP solution and stained with DAPI. The number of sperm adhered to an oocyte was determined by counting DAPI-positive sperm on an oocyte.

Membrane localization of β-catenin before and after membrane adhesion. To observe the localization of β-catenin before and after membrane adhesion, oocytes were collected as mentioned in the 'Determination of litter size and IVF' section. After ZP removal, 'zona-free' oocytes were incubated with C57BL/6N epididymal sperm (ca. 1.5×10^5 sperm/ml) in a 30-μl drop of TYH medium for 30 min at 37°C. The oocytes adhered to sperm, oocytes before sperm adhesion, and epididymal sperm were fixed by placing them in PFA-GLA-PVP solution, washed, and immunostained with a mAb against β-catenin and DAPI, as described in the 'Immunostaining' section.

IVF of oocytes treated with UBE1-41. To study the effect of UBE1-41 on sperm-oocyte fusion, oocytes were collected as mentioned in the 'Determination of litter size and IVF' section, incubated in a 30-μl drop of TYH medium containing UBE1-41 (Biogenova) and DAPI for 1 h at 37°C, and washed with TYH medium. After ZP removal, 'zona-free' oocytes (30 oocytes) were incubated with C57BL/6N epididymal sperm (ca. 1.5×10^5 sperm/ml) in a 30-μl drop of TYH medium for 30 min at 37°C. These oocytes were then fixed by placing them in PFA-GLA-PVP solution, washed, and immunostained with a mAb against β-catenin, as described in the 'Immunostaining' section. The 'zona-free' oocytes were similarly treated in a medium without UBE1-41 and used as the control. The relative rate of oocytes fused with sperm was compared between UBE1-41-treated and untreated oocytes.

1. Ikawa, M., Inoue, N., Benham, A. M., and Okabe, M. Fertilization: a sperm's journey to and interaction with the oocyte. *J Clin Invest* **120**, 984–994 (2010).
2. Mitamura, T. *et al.* The 27-kD diphtheria toxin receptor-associated protein (DRAP27) from vero cells is the monkey homologue of human CD9 antigen: expression of DRAP27 elevates the number of diphtheria toxin receptors on toxin-sensitive cells. *J Cell Biol* **118**, 1389–1399 (1992).
3. Inoue, N., Ikawa, M., Isotani, A., and Okabe, M. The immunoglobulin superfamily protein Izumo is required for sperm to fuse with eggs. *Nature* **434**, 234–238 (2005).
4. Miyado, K. *et al.* Requirement of CD9 on the egg plasma membrane for fertilization. *Science* **287**, 321–324 (2000).
5. Le Naour, F. *et al.*, Severely reduced female fertility in CD9-deficient mice. *Science* **287**, 319–321 (2000).
6. Miyado, K. *et al.* The fusing ability of sperm is bestowed by CD9-containing vesicles released from eggs in mice. *Proc Natl Acad Sci USA* **105**, 12921–12926 (2008).
7. Barraud-Lange, V. *et al.* Transfer of oocyte membrane fragments to fertilizing spermatozoa. *FASEB J* **21**, 3446–3449 (2007).
8. Runge, K. E. *et al.* Oocyte CD9 is enriched on the microvillar membrane and required for normal microvillar shape and distribution. *Dev Biol* **304**, 317–325 (2007).
9. Yamada, S. *et al.* Deconstructing the cadherin-catenin-actin complex. *Cell* **123**, 889–901 (2005).
10. De Vries, W. N. *et al.* Maternal beta-catenin and E-cadherin in mouse development. *Development* **131**, 4435–4445 (2004).
11. Nagafuchi, A., Ishihara, S., and Tsukita, S. The roles of catenins in the cadherin-mediated cell adhesion: functional analysis of E-cadherin-alpha catenin fusion molecules. *J Cell Biol* **127**, 235–245 (1994).
12. Behrens, J. *et al.* Functional interaction of beta-catenin with the transcription factor LEF-1. *Nature* **382**, 638–642 (1996).
13. Fulka, J., Jr., Flechon, B., and Flechon, J. E. Fusion of mammalian oocytes: SEM observations of surface changes. *Reprod Nutr Dev* **29**, 551–557 (1989).

14. Takeichi, M. The cadherins: cell-cell adhesion molecules controlling animal morphogenesis. *Development* **102**, 639–655 (1988).
15. Ziv, S., Rufas, O., and Shalgi, R. Cadherins expression during gamete maturation and fertilization in the rat. *Mol Reprod Dev* **62**, 547–556 (2002).
16. Bedford, J. M., Mori, T., and Oda, S. The unusual state of the cumulus oophorus and of sperm behaviour within it, in the musk shrew, Suncus murinus. *J Reprod Fertil* **110**, 127–134 (1997).
17. Boussadia, O. *et al.* E-cadherin is a survival factor for the lactating mouse mammary gland. *Mech Dev* **115**, 53–62 (2002).
18. Brault, V. *et al.* Inactivation of the beta-catenin gene by Wnt1-Cre-mediated deletion results in dramatic brain malformation and failure of craniofacial development. *Development* **128**, 1253–1264 (2001).
19. Vasioukhin, V. *et al.* Hyperproliferation and defects in epithelial polarity upon conditional ablation of alpha-catenin in skin. *Cell* **104**, 605–617 (2001).
20. Le, T. L., Yap, A. S., and Stow, J. L. Recycling of E-cadherin: a potential mechanism for regulating cadherin dynamics. *J Cell Biol* **146**, 219–232 (1999).
21. Aberle, H. *et al.* Beta-catenin is a target for the ubiquitin-proteasome pathway. *EMBO J* **16**, 3797–3804 (1997).
22. Molfetta, R. *et al.* Lipid raft-dependent FcepsilonRI ubiquitination regulates receptor endocytosis through the action of ubiquitin binding adaptors. *PLoS One* **4**, e5604 (2009).
23. Granell, S., Mohammad, S., Ramanagoudr-Bhojappa, R., and Baldini, G. Obesity-linked variants of melanocortin-4 receptor are misfolded in the endoplasmic reticulum and can be rescued to the cell surface by a chemical chaperone. *Mol Endocrinol* **24**, 1805–1821 (2010).
24. Daniel, J. M. and Reynolds, A. B. The tyrosine kinase substrate p120cas binds directly to E-cadherin but not to the adenomatous polyposis coli protein or alpha-catenin. *Mol Cell Biol* **15**, 4819–4824 (1995).
25. Brind, S., Swann, K., and Carroll, J. Inositol 1,4,5-trisphosphate receptors are downregulated in mouse oocytes in response to sperm or adenophostin A but not to increases in intracellular Ca(2+) or egg activation. *Dev Biol* **223**, 251–265 (2000).
26. Bowerman, B. and Kurz, T. Degrade to create: developmental requirements for ubiquitin-mediated proteolysis during early C. elegans embryogenesis. *Development* **133**, 773–784 (2006).
27. Cheon, S. S. *et al.* beta-Catenin stabilization dysregulates mesenchymal cell proliferation, motility, and invasiveness and causes aggressive fibromatosis and hyperplastic cutaneous wounds. *Proc Natl Acad Sci U S A* **99**, 6973–6978 (2002).
28. Kimura, T. *et al.* The stabilization of beta-catenin leads to impaired primordial germ cell development via aberrant cell cycle progression. *Dev Biol* **300**, 545–553 (2006).
29. Coutifaris, C. *et al.* E-cadherin expression during the differentiation of human trophoblasts. *Development* **113**, 767–777 (1991).
30. Deli, M. A. Potential use of tight junction modulators to reversibly open membranous barriers and improve drug delivery. *Biochim Biophys Acta* **1788**, 892–910 (2009).
31. Jegou, A. *et al.* CD9 tetraspanin generates fusion competent sites on the egg membrane for mammalian fertilization. *Proc Natl Acad Sci U S A* **108**, 10946–10951 (2011).
32. Gamallo, C. *et al.* Correlation of E-cadherin expression with differentiation grade and histological type in breast carcinoma. *Am J Pathol* **142**, 987–993 (1993).
33. Choi, Y. H. and Toyoda, Y.. Cyclodextrin removes cholesterol from mouse sperm and induces capacitation in a protein-free medium. *Biol Reprod* **59**, 1328–1333 (1998).
34. Sakakibara, K. *et al.* Molecular identification and characterization of Xenopus egg uroplakin III, an egg raft-associated transmembrane protein that is tyrosine-phosphorylated upon fertilization. *J Biol Chem* **280**, 15029–15037 (2005).
35. Jones-Villeneuve, E. M., McBurney, M. W., Rogers, K. A., and Kalnins, V. I.. Retinoic acid induces embryonal carcinoma cells to differentiate into neurons and glial cells. *J Cell Biol* **94**, 253–262 (1982).
36. Sato, K. *et al.* Low density detergent-insoluble membrane of Xenopus eggs: subcellular microdomain for tyrosine kinase signaling in fertilization. *Development* **129**, 885–896 (2002).
37. de Vries, W. N. *et al.* Expression of Cre recombinase in mouse oocytes: a means to study maternal effect genes. *Genesis* **26**, 110–112 (2000).

Acknowledgements

We thank W.N. de Vries and B.B. Knowles for the Zp3-Cre transgenic mice. This work was supported by a grant from The Ministry of Health, Labor and Welfare, and grant-in-aid for Scientific Research, The Ministry of Education, Culture, Sports, and Technology of Japan.

Author Contributions

KM conceived and designed the experiments. YT, KY, MS, AN, NK, KS, TK, YH, NO, SK, and MM performed the experiments. HS, YT, HA, and AU analyzed the data. KM wrote the main manuscript text and prepared figures. All authors reviewed the manuscript.

Additional information

Supplementary Information accompanies this paper at http://www.nature.com/scientificreports

Competing financial interests: The authors declare no competing financial interests.

How to cite this article: Takezawa, Y. *et al.* β-catenin is a molecular switch that regulates transition of cell-cell adhesion to fusion. *Sci. Rep.* **1**, 68; DOI:10.1038/srep00068 (2011).

Biochemical and Biophysical Research Communications 410 (2011) 351–357

Contents lists available at ScienceDirect

Biochemical and Biophysical Research Communications

journal homepage: www.elsevier.com/locate/ybbrc

Innate immune system still works at diapause, a physiological state of dormancy in insects

Akihiro Nakamura [a,1], Kenji Miyado [a,*,1], Youki Takezawa [a], Naoko Ohnami [a], Masahiro Sato [b], Chihiro Ono [a], Yuichirou Harada [a], Keiichi Yoshida [a], Natsuko Kawano [a], Seiya Kanai [a], Mami Miyado [a], Akihiro Umezawa [a]

[a] Department of Reproductive Biology, National Center for Child Health and Development, 2-10-1 Okura, Setagaya, Tokyo 157-8535, Japan
[b] Section of Gene Expression Regulation, Frontier Science Research Center, Kagoshima University, 1-21-20 Korimoto, Kagoshima 890-0065, Japan

ARTICLE INFO

Article history:
Received 25 May 2011
Available online 7 June 2011

Keywords:
Innate immune system
Diapause
Hemocyte
Insect
Pupae
Dormancy

ABSTRACT

Diapause is most often observed in insects and is a physiologically dormant state different from other types of dormancy, such as hibernation. It allows insects to survive in harsh environments or extend longevity. In general, larval, pupal, or adult non-diapausing insects possess an innate immune system preventing the invasion of microorganisms into their bodies; however, it is unclear whether this system works under the dormant condition of diapause. We here report the occurrence of innate cellular reactions during diapause using pupae of a giant silkmoth, *Samia cynthia pryeri*. Scanning electron microscopic analysis demonstrated the presence of two major types of cells in the body fluid isolated from the thoracic region of a pupa. Phagocytosis and encapsulation, characteristics of innate cellular reactions, by these cells were observed when latex beads as foreign targets were microinjected into the internal portion of a pupa. Such behavior by these cells was still observed even when pupae were continuously chilled at 4 °C. Our results indicate that innate cellular reactions can work in diapausing insects in a dormant state.

1. Introduction

Insects have evolved a diverse strategy of diapause that occurs at the embryonic, larval, pupal, or adult stage, depending on the species [1]. Initiation of diapause in insects is controlled by different mechanisms, depending on their developmental stage. For example, pupal diapause is regulated by the absence or presence of prothoracicotropic hormone, an insect neurohormone, released from the brain [1]. Adult diapause is induced when juvenile hormone, a hormone secreted by secretory glands located near the brain, is deficient, while larval diapause is induced by juvenile hormone [2]. Once diapause occurs, the respiratory activity of insects drops markedly and the lowered activity is maintained at a minimum level, under which the insects are able to survive for months or even years [3].

In insects, the innate immune system generally consists of humoral and cellular defense reactions [4]. Since this system is a characteristic of plants, fungi, insects, and primitive multicellular organisms (but not for mammals), it has long been considered an evolutionarily older defense system [4]. However, the recent discovery of Toll-like receptors in both insects and mammals provided a new insight into the role of innate immunity as a skillful system for preventing the invasion of microorganisms into the body [5]. The humoral defense reactions are mediated by (1) production of anti-microbial peptides, (2) stimulation of cascades that regulate coagulation and melanization of hemolymph, a body fluid circulating within an insect body like blood in mammals, and (3) production of reactive intermediates of oxygen and nitrogen [6].

Since hemocytes that are similar to blood cells in mammals are known to be present in many insects, such as the silkmoth, *Bombyx mori*, fruit fly, *Drosophila melanogaster*, desert locust, *Schistocerca gregaria*, and sphinx moth, *Manduca sexta*, they are believed to play roles in the innate immune system [7]. Cellular defense reactions, such as "phagocytosis" and "encapsulation" are preceded by two different types of hemocytes, depending on the insect species [7]. For instance, in *Lepidoptera*, granulocytes and plasmatocytes are involved in the reactions, whereas in *Drosophila*, plasmatocytes and lamellocytes are involved [7]. Insect hemocytes can not only recognize and eliminate a variety of foreign targets, but also alter part of their own tissues during metamorphosis, a biological phenomenon required for developing to the next stage in insects [8]. Similarly, in amphibians and mammals, immune cells participate in tissue regeneration by eliminating damaged cells [9]. Several lines of evidence have demonstrated that humoral and cellular defense reactions work coordinately [10]. In addition, cross-talk between the immune and nervous systems is thought to

* Corresponding author. Fax: +81 3 5494 7048.
E-mail address: kmiyado@nch.go.jp (K. Miyado).
[1] These authors equally contributed to this work.

0006-291X/$ - see front matter © 2011 Elsevier Inc. All rights reserved.
doi:10.1016/j.bbrc.2011.06.015

be important for regulating inflammation-like reactions upon microbial infection [11]; however, little is known about hemocyte-mediated cellular defense reactions at diapause. In this study, we explored the above possibility using diapausing pupae of a giant moth, *Samia cynthia pryeri*, inhabiting a field.

2. Materials and methods

2.1. Animals

Fifty diapausing pupae of *S. cynthia pryeri* (about 2 months after pupation) were collected from an outdoor rearing location in a field near Matsumoto city (Nagano, Japan) in early December, and stored in an incubator at 4 °C until used for experiments. Since a male pupa is bigger than a female pupa, the former is superior for isolation of a relatively large amount of body fluid (in which innate immunity-related cells are supposed to be included) than the latter. Based on this reason, we used male pupae (3–5 months after pupation) throughout the following experiments.

2.2. Identification of hemocyte-like cells in diapausing pupae

Hemocyte-like cells were identified as described in supplementary content.

2.3. Determination of respiration rates in diapausing pupae

Respiration rates were measured as described in supplementary content.

2.4. Analysis by scanning electron microscopy (SEM)

Hemolymph collected from a diapausing pupa was observed as described in supplementary content.

2.5. Injection of latex beads into diapausing pupae

To monitor the behavior of innate immunity-related cells probably present within diapausing pupae, microinjection experiments were performed as described in supplementary content.

3. Results

3.1. Life cycle of S. cynthia pryeri

The Ailanthus silkmoth, *S. cynthia*, is a saturniid moth used to produce silk fabric, but is not so domesticated as the silkworm, *B. mori*. In Japan, a subspecies of *S. cynthia* exists and is named *S. cynthia pryeri*. This insect is often called "eri-silkmoth" as its common name, because it feeds on the leaves of the castor bean and produces eri-silk. The name 'eri' is derived from the Assamese word 'era', which means castor. Eri-silk is extremely durable, but cannot be easily reeled off the cocoon and is thus spun like cotton or wool. Under cold climatic conditions (from November to June), *S. cynthia pryeri* sleep as a diapausing pupa and then develop to a moth in early summer (Fig. 1A). The moth has very large wings, 113–125 mm in length, with whitish and yellow stripes against a brown background (Fig. 1B). The pupa does not change its morphology or weight during the long diapausing period, and males are larger than females (Fig. 1C).

Under laboratory conditions, diapausing pupae can survive for over a year without awakening from diapause, as long as they are continuously stored at 26 °C. For development of a pupa to a moth, the diapausing pupa must be exposed to low temperature (under 4 °C) for over 90 days and subsequently warmed at 26 °C. As shown in Fig. 1D, in pupae exhibiting complete diapause, transient spike-like CO_2 discharge is seen, indicating that their metabolic activity drops markedly and their dormant condition is properly maintained. In this study, male pupae exhibiting a spike-like respiration pattern were defined as those in complete diapause and were used in the following experiments.

3.2. Presence of innate immunity-related cells in diapausing pupae

To assess possible evidence for the occurrence of innate immune reactions at diapause, we first explored the presence of cells that appear to be similar to hemocytes in diapausing pupae of *S. cynthia pryeri*. Prior to this investigation, we selected diapausing pupae exhibiting complete diapause. Since the respiratory activity of a pupa reaches the minimum level by 15 days after pupation (initiation of cocoon formation), it is thought that stable diapause is achieved more than 15 days after pupation; therefore, we used diapausing pupae 90–150 days after pupation in this experiment. Furthermore, it is important to know where hemocytes reside within a diapausing pupa. Hemocytes are thought to not only be involved in cellular defense reactions, but also in tissue formation via metamorphosis [8]. Based on this knowledge, we supposed that pupal hemocytes reside around immature organs, such as wing imaginal discs, to participate in the forthcoming metamorphosis after diapause. We thus collected body fluid from the thoracic region of diapausing pupa where wing imaginal discs are located (Fig. 2A). Light microscopic observation of cellular content included in the collected body fluid revealed that all (10 tested) of the diapausing pupae had cells free from tissues (Fig. 2B). These cells were divided into two major types: Type I cells (arrows in Fig. 2B) were ca. 10 μm in diameter, round and less adhesive, and exhibited low migrating ability; Type II cells (arrowheads in Fig. 2B) were more than 20 μm in diameter, flat and adhesive, and exhibited high migrating ability. The rates of Type I and II cells in the collected body fluid were 47.3 ± 1.8% and 46.8 ± 2.2%, respectively (Fig. 2C). In addition to these two types of cells, there was a minor type of sticky cell (ca. 10 μm in diameter) that was categorized as "others" in Fig. 2C.

To examine these two cell types in more detail, we performed SEM analysis. As already noted from light microscopic analysis, there were two distinct types of cells. One exhibited round morphology and protruding microvillar processes (upper panels of Fig. 2D), corresponding to Type I cells (arrows in Fig. 2B) observed under a light microscope. The other exhibited flattened morphology and extended peripheral waves similar to lamellipodia (lower panels of Fig. 2D), corresponding to the previous Type II cells (arrowheads in Fig. 2B). Type I cells (9.0 ± 0.3 μm) were smaller than Type II cells (26.8 ± 1.0 μm) in average diameter. These Type I and II cells shared morphological features with granulocytes and plasmatocytes, respectively, identified as insect hemocytes in a sphinx moth, *M. sexta* [7]. These results indicate the presence of at least two types of cells similar to hemocytes in the diapausing pupae of *S. cynthia pryeri*.

3.3. Responses of hemocyte-like cells to foreign latex beads in vivo

As mentioned previously, two cell types similar to hemocytes were found in a diapausing pupa of *S. cynthia pryeri*. To examine whether these cells exhibit defensive ability against foreign invaders, latex beads were microinjected as a target of the cellular reaction into the right side of the thoracic ventral region of a pupa incubated at 20 °C using a glass microcapillary, as depicted in Fig. 3A. Six hours after injection, the injected beads were recovered by suctioning the internal body fluid (10 μl) through the left side of the thoracic ventral region of the bead-injected pupa using a glass

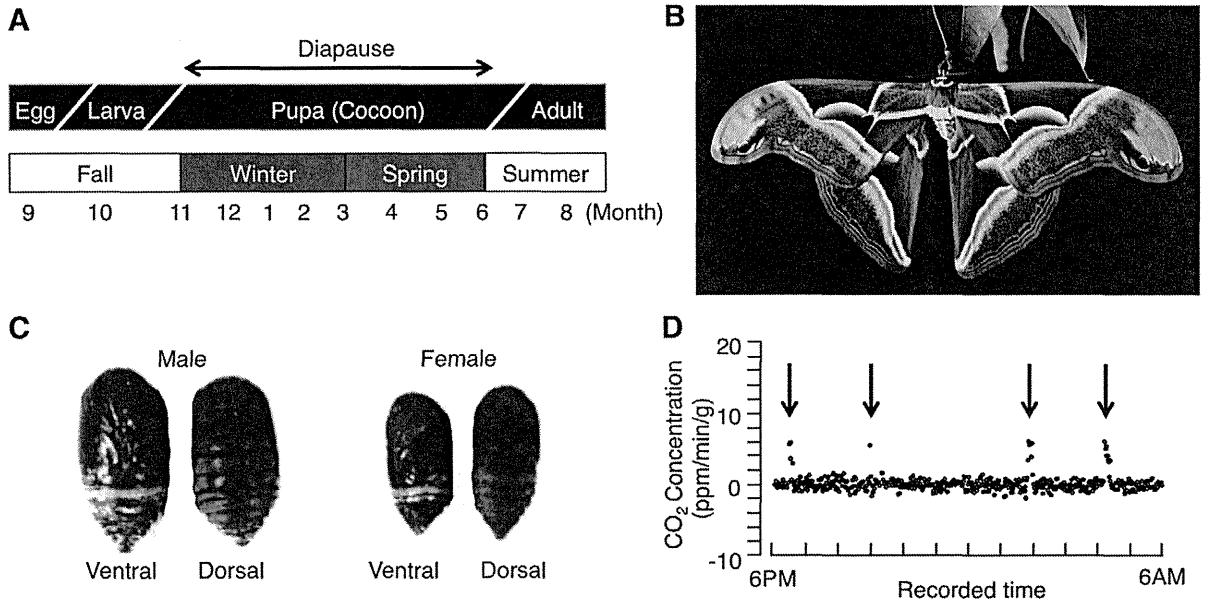

Fig. 1. Features of diapausing pupae of a giant moth, *Samia cynthia pryeri*. (A) Life cycle of the insect. The most common life cycle is univoltine, in which this moth takes one year to complete its life, winters as a diapausing pupa, and then develops to an adult in early summer. Notably, the pupa spends more than 6 months in diapause. (B) Male moth. The moth has large wings (ca. 120 mm in width) with whitish stripes and a brown background on both the upper and lower wings. (C) Diapausing pupae. Left image: male pupa; right image: female pupa. (D) Representative pattern of transient, spike-like CO_2 discharge (indicated by arrows) in the diapausing pupa 30 days after pupation. Periodic appearance of spike-like CO_2 discharge indicates a marked decrease in metabolic activity and normal diapausing conditions.

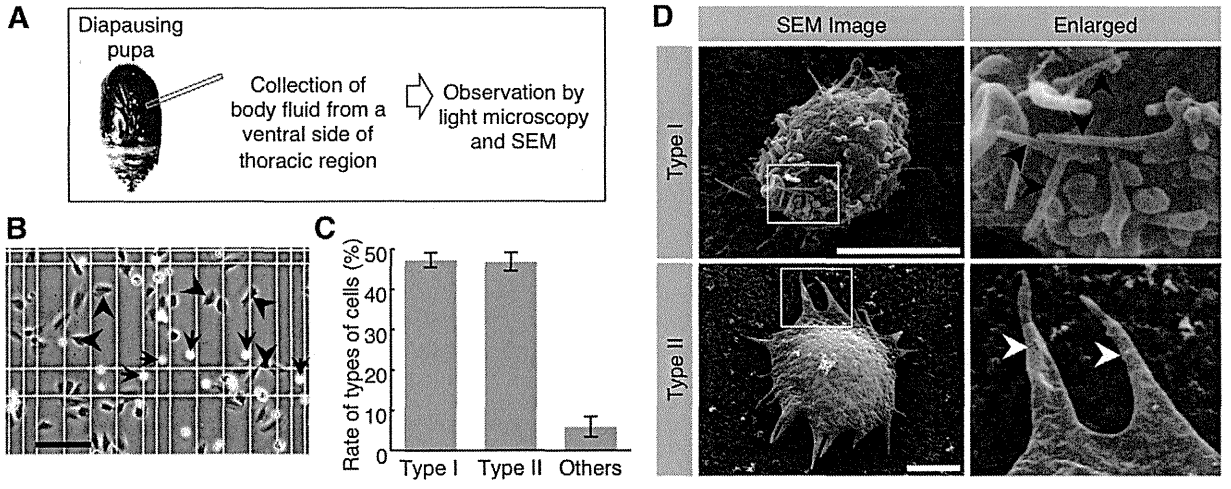

Fig. 2. Discovery of hemocyte-like cells in diapausing pupae. (A) Experimental design. Since pupal hemocytes were predicted to reside around wing imaginal discs, body fluid was collected for microscopic analysis from thoracic regions that house wing imaginal discs. (B) Hemocyte-like cells present in the body fluid collected from the thoracic region of a pupa. Arrows and arrowheads indicate Type I and II cells, respectively. Scale bars: 50 μm. (C) Rate of hemocyte-like cells (classified as Type I, Type II and others) in body fluids collected from the thoracic region shown in B. Over 2000 cells were counted. The rate of each cell type is determined and expressed as a percentage of a target cell type among the total number of cells counted in ten quadrants (1 mm × 1 mm in square). Values are the mean ± standard error (SE). (D) SEM analysis of migrating cells in the diapausing pupae of *Samia cynthia pryeri*. The migrating cells collected from the thoracic region of diapausing pupae of *Samia cynthia pryeri* were subjected to SEM analysis. Right panels are enlarged images of insets in the left panels. Black arrowheads: microvillus-like structures elongated from Type I cells; white arrowheads: lamellipodia-like structures extended from Type II cells. Scale bars: 10 μm.

microcapillary. The cellular content included in the recovered body fluid was then subjected to SEM analysis (Fig. 3B–E).

As expected, the two cell types shown in Fig. 2D were seen in the cellular content (marked by arrowhead and asterisks in Fig. 3B). Notably, only one (marked by asterisks) of the two cell types exhibited phagocytotic behavior toward the foreign beads (Fig. 3C). In some cases, two or more cells were engulfing a bead (Fig. 3D). These cells exhibited round morphology with microvilli and their average diameter was ca. 10 μm (Fig. 3B–D). These features clearly match those of Type I cells, shown in Fig. 2D. On the other hand, the capsule was detected in the cellular content (Fig. 3E). Since *Lepidoptera* granulocytes and plasmatocytes are involved in encapsulation [7], another type of lamellipodial cell, morphologically similar to plasmatocytes [7], is supposed to exhibit behavior (namely, encapsulation) different from that of Type I cells (Fig. 3E). These cells have a larger diameter and flat cell surface, suggesting a feature of the Type II cells shown in Fig. 2D. Concomitantly, hemolymph containing injected beads was smeared on the glass slides for Giemsa staining. Similar to the findings obtained from SEM analysis, phagocytosis (Fig. 3F) and encapsulation

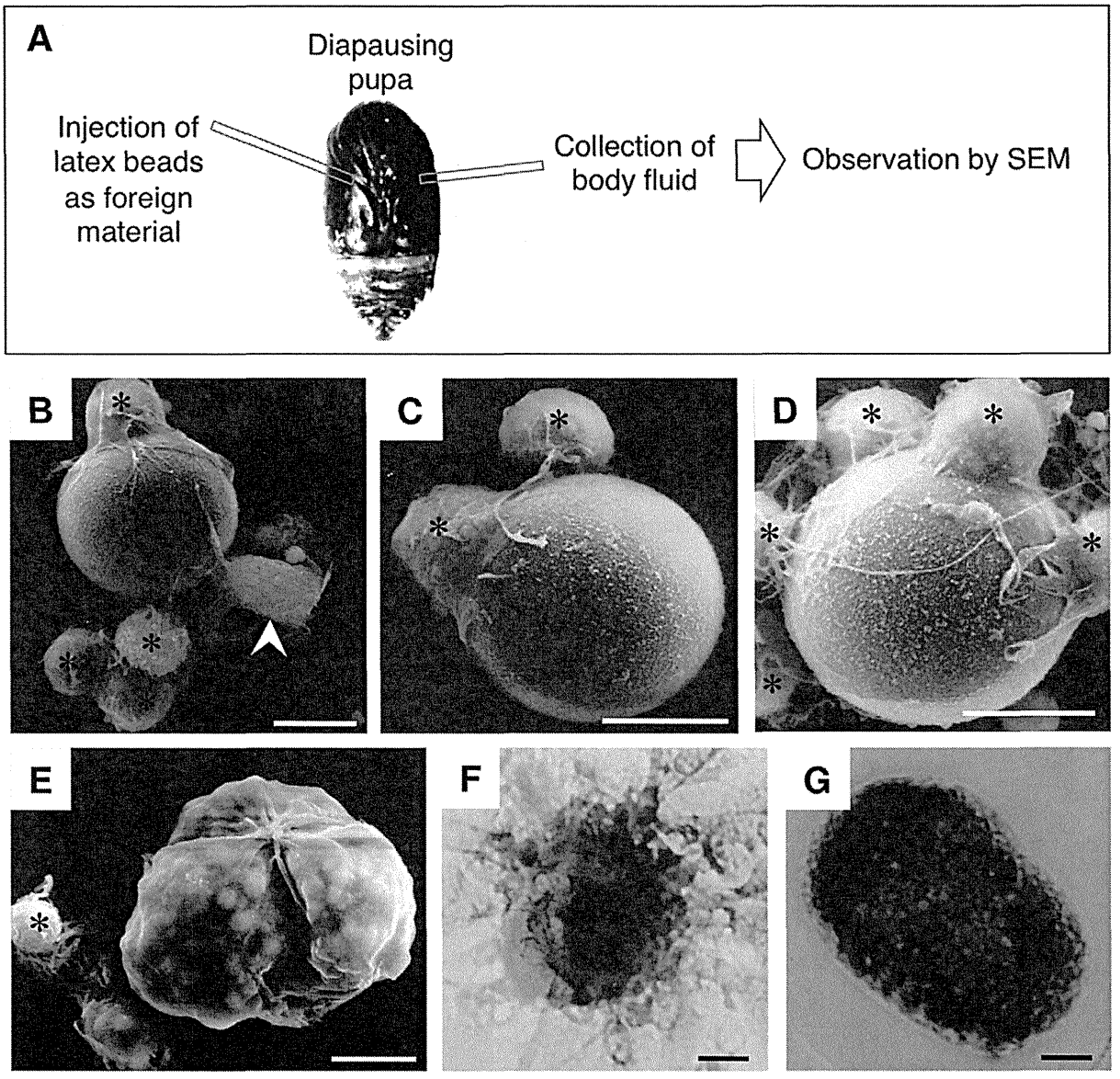

Fig. 3. Innate immune reactions as revealed by microinjection of foreign latex beads into diapausing pupae of *Samia cynthia pryeri*. (A) Experimental design. To assess the behavior of hemocyte-like cells toward foreign targets, latex beads were microinjected into the right side of the thoracic ventral region of a pupa incubated at 20 °C using a glass microcapillary. Six hours after injection, the beads were recovered by suctioning the body fluid from the left side of the thoracic ventral region. (B) Two types of hemocyte-like cells adhered to the injected latex bead. Black asterisks and white arrowhead indicate Type I and II cells, respectively. (C) Type I cells (indicated by asterisks) displaying phagocytotic behavior against the bead. (D) Five Type I cells (indicated by asterisks) displaying phagocytotic behavior against the bead. (E) Type II cells encapsulating bead. Type I cells (indicated by asterisks) are present near the encapsulated bead. (F) Giemsa staining indicating phagocytosis by Type I cells. Note the presence of Type I cells stained blue surrounding the black bead. (G) Giemsa staining indicating encapsulation by Type II cells. Note that the black bead is completely surrounded by blue-stained Type II cells. Scale bars: 10 μm.

(Fig. 3G) were observed. From these collective results, migrating cells found in a diapausing pupa have defensive abilities, as exemplified by their phagocytosis and encapsulation, suggesting that innate cellular reactions work even in diapause.

3.4. Cellular responses under low-temperature

During the winter season where *S. cynthia pryeri* inhabits, the outdoor temperature is usually below 0 °C throughout the day. As a result, microorganisms such as bacteria and fungi become metabolically inactive, although they are still alive and can grow slowly [12]. Furthermore, they often suffer from bacterial invasion [13]; however, it is still unknown whether the innate immune system works in diapausing pupae exposed to low temperature (4 °C or below).

To assess the question, we examined the defensive ability of diapausing pupae stored at 4 °C by microinjecting latex beads into their internal lumen, as depicted in Fig. 3A. After injection, the injected beads were recovered by sucking out the body fluid each hour and subjecting it to Giemsa staining to identify innate immunity-related cells. In pupae incubated at 20 °C, phagocytosis by Type I cells was observed in all the samples tested, which had been collected up to 5 h after bead injection. Furthermore, the number of beads phagocytosed increased in a time-dependent manner (upper left graph in Fig. 4). In pupae incubated at 4 °C, phagocytosis was still observed, but the frequency was lower than in pupae incubated at 20 °C (upper right graph in Fig. 4). In contrast, the average rates of encapsulation were below 10% in both groups when samples were examined up to 5 h after bead injection (mid-

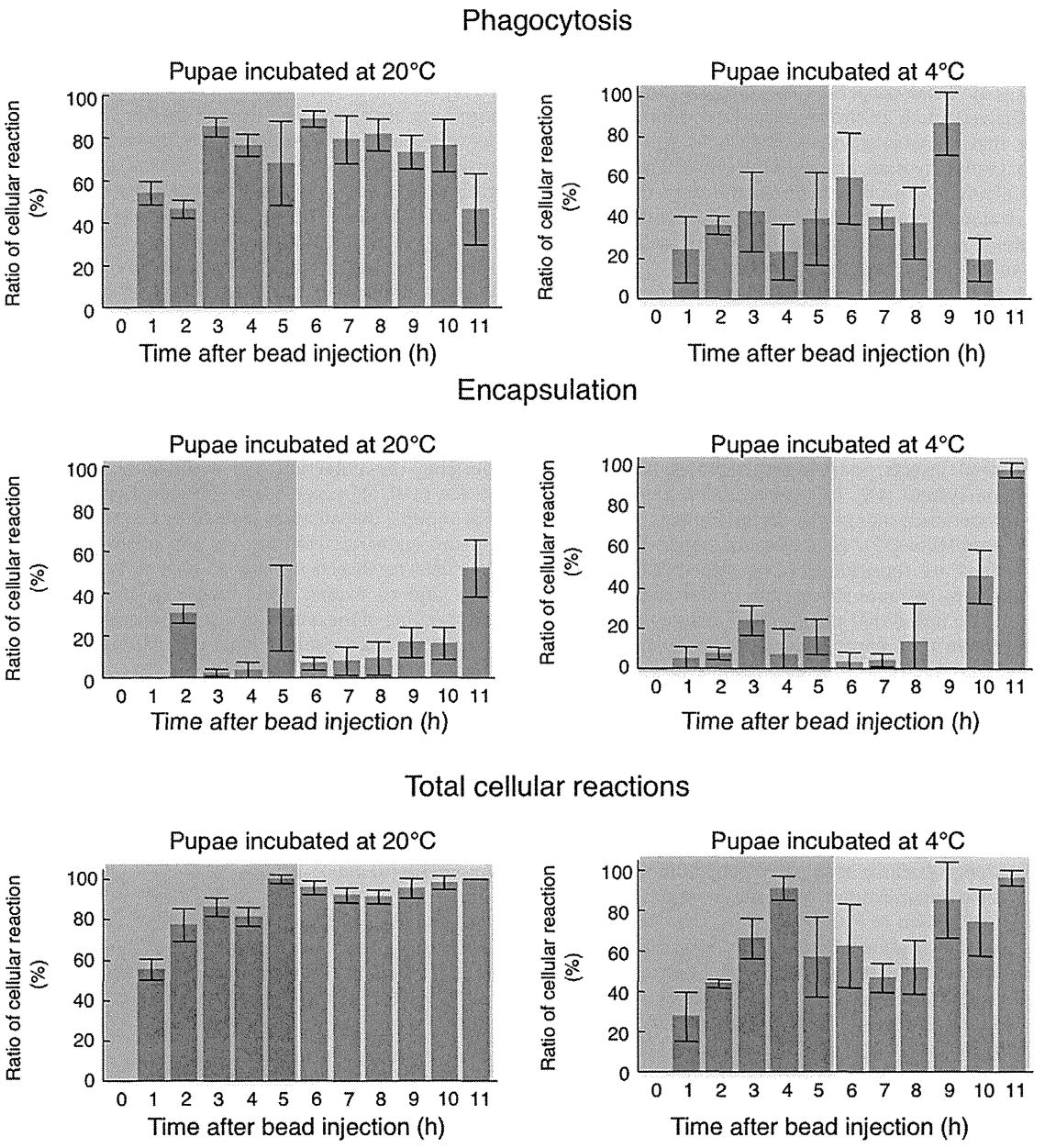

Fig. 4. Cellular defense reactions in diapausing pupae incubated at two different temperatures. As depicted in A, latex beads were microinjected into the right side of thoracic ventral region of a diapausing pupa incubated at 4 or 20 °C, and then the injected beads were recovered from the left side of the thoracic ventral region each hour after bead injection. Phagocytosis and encapsulation were evaluated by inspecting specimens after Giemsa staining. The rate of each cellular defense reaction was determined as described in Fig. 2C. Total cellular reactions were determined by the sum of the rates of phagocytosis and encapsulation.

dle graphs in Fig. 4). The degree of total cellular reactions in the group treated at 4 °C was low compared to the group treated at 20 °C (lower graphs in Fig. 4). These results suggest that the innate immunity associated with phagocytosis and encapsulation is affected by temperature outside the insect bodies.

Similar results were obtained when phagocytotic activities were evaluated 6–11 h after bead injection (upper graphs in Fig. 4). Notably, the encapsulation rate tended to gradually increase in pupae incubated at 4 °C and reached at the maximal level of 95.0 ± 0.4% at 11 h after bead injection. This is in contrast with the rate (50.0 ± 0.6%) in pupae incubated at 20 °C (middle graphs in Fig. 4). These results suggest that the phagocytotic activity of Type I cells is affected by outside temperature, while encapsulation by Type II cells proceeds even at low temperature (4 °C). This means that innate cellular reactions still work in diapausing pupae exposed to low temperature.

4. Discussion

Insects overcome harsh environmental conditions, such as food shortages and extremely low or high temperatures, by employing a unique system, termed diapause [1]. For example, in the case of pupal diapause, at which stage food sources are unavailable, managing the metabolic resources stored in their bodies is critical for their survival [1]. Metabolic depression, as represented by spike-like respiration (shown in Fig. 1D), is one of the strategies for insects to promote reserve conservation [1]. Diapausing insects also

have to control water loss, since they are unable to take in water, especially in the winter season. The body fluid of diapausing insects in this season is viscous and rich in anti-freezing materials, such as glycerol [14]. These properties may protect insects from environmental changes, such as chilling and water shortage. It is also conceivable that diapausing insects may have strategies to protect against bacterial invasion, although the self-defense mechanism remains unknown. Our present study addressed this problem and demonstrated using diapausing pupae of *S. cynthia pryeri* that cellular defense reactions work in diapausing pupae constantly exposed to chilling temperature.

There is much evidence that insects exhibit their immune competence in a non-diapausing state. For example, in non-diapausing adults of *D. melanogaster*, temperature-induced changes in immune competence are accompanied with cell surface alterations that cause their hemocytes to adhere and encapsulate a parasite [15]. At 29 °C, the hemocytes can encapsulate eggs of the parasitic wasp, but they are essentially immune incompetent at 21 °C [15]. In addition to terrestrial insects, marine invertebrates have their own innate immune system [16]. In sea cucumber, *Apostichopus japonicus*, acute temperature change significantly affects phagocytosis, but not encapsulation [17]. This evidence suggests that innate cellular reactions are sensitive to temperature change, and phagocytosis appears to be more susceptible to this change than encapsulation. We also noted that phagocytosis is more susceptible to low temperature than encapsulation in diapausing pupae of *S. cynthia pryeri* (see Fig. 4).

Bead injection into the internal portion of a pupa has been proven as a simple and effective approach to evaluate cellular immune reactions *in vivo* [18]. This direct approach is particularly valuable when the genetic background and species of the target samples is unknown. In this case, the collected body fluid containing injected beads was always analyzed by electron microscopy, such as SEM; however, SEM is labor-intensive and requires a relatively long time to obtain results. Giemsa staining of smeared body fluid was found to be useful for rapid identification of innate immunity-related cells in this study, as shown in Fig. 3F, G. Thus, Giemsa staining would be beneficial for routine identification of innate immunity-related cells recovered after bead injection. Flow cytometric analysis is also a useful alternative to identify and purify blood cells of various animals, including *D. melanogaster* [19]. For this, it requires specific lectins or antibodies recognizing those cells. In fact, lectin-like substances with hemagglutinating activity have been found in the hemolymph of a variety of insect species [8]. In some insects, lectin-binding patterns correlate with the immune capabilities of the hemocytes [20]. Unfortunately, neither lectin nor an antibody that specifically recognizes hemocytes derived from *S. cynthia pryeri* is available.

The number of hemocytes has been estimated in diapausing and non-diapausing larvae of the greater sugar cane borer, *Sesamia cretica* [21]. During diapause, the number of each type of hemocyte is significantly reduced, but it increases along with termination of diapause, suggesting the possible incompetence of innate cellular reactions at diapause [21]. However, our present results obtained from injecting latex beads demonstrated that cellular defense reactions continue to function in diapausing pupae of *S. cynthia pryeri*. This indicates that the activity of the innate cellular system is reduced in diapause, but is maintained.

SEM analysis of cells included in body fluid of diapausing *S. cynthia pryeri* demonstrated the presence of two major types of hemocytes, termed Type I and II cells. Minor types of cells (ca. 10 μm in diameter), which are sticky and categorized as "others" in Fig. 2C, were also detected. The morphological features of Type I cells are similar to those of granulocytes in *Lepidoptera* [7]. Granulocytes are known to differentiate into other types of cells [22]. Probably, the minor types of cells mentioned above are derived from Type I cells.

To date, the presence of seven subpopulations of hemocytes has been reported in several insect species, but not all of these subpopulations are always present in each species [7]. The most common types of hemocytes are prohemocytes, plasmatocytes, granulocytes, spherulocytes, adipocytes, and oenocytoids, although each cell type slightly differs among species. Notably, close similarity of immunological functions has been demonstrated between vertebrate leukocytes and insect hemocytes [23]. For example, prohemocytes, plasmatocytes and granulocytes are thought to correspond to lymphocytes, monocytes and neutrophils in humans, respectively [23]. The kinetics of phagocytosis and microbial killing is similar between insects and humans [23]. For precise characterization of the hemocyte subpopulation, the development of appropriate cell surface markers for segregating each type of hemocyte subpopulation will be required.

At present, little is known about the molecular mechanism underlying the induction and maintenance of insect diapause. Emerson et al. [1] suggest that the induction and maintenance of larval or pupal diapause are under direct control of the insect brain via neuro-endocrine complex. As previously mentioned, diapause is beneficial for insects to survive under severe environmental conditions and to extend their longevity. In this context, further understanding of the nature of insect diapause will provide new insight into studies on human longevity, pathogenesis and the development of therapeutic drugs.

In conclusion, we show for the first time using a bead injection method into the internal portion of a pupa that cellular defense reactions work even in diapausing pupae of *S. cynthia pryeri*, which are continuously exposed to chilling temperature. This finding would be useful to further understand the role of hemocytes in insect innate immunity.

Acknowledgments

We thank A. Koenuma, K. Mizukoshi, Y. Shinohara, S. Kobayashi and T. Shimada for critical suggestions. This work was supported by a grant from the Ministry of Health, Labor and Welfare, and a grant-in-aid for Scientific Research from the Ministry of Education, Culture, Sports, and Technology of Japan.

Appendix A. Supplementary data

Supplementary data associated with this article can be found, in the online version, at doi:10.1016/j.bbrc.2011.06.015.

References

[1] K.J. Emerson, W.E. Bradshaw, C.M. Holzapfel, Complications of complexity: integrating environmental, genetic and hormonal control of insect diapause, Trends Genet. 25 (2009) 217–225.
[2] H. Numata, S. Nakayama, J. Matsuo, Role of the corpus allatum in the control of adult diapause in the blow fly, Protophormia terraenovae, J. Insect Physiol. 43 (1997) 211–216.
[3] L. Ding, Y. Li, M. Goto, Physiological and biochemical changes in summer and winter diapause and non-diapause pupae of the cabbage armyworm, Mamestra brassicae L. during long-term cold acclimation, J. Insect Physiol. 49 (2003) 1153–1159.
[4] D. Hultmark, Immune reactions in Drosophila and other insects: a model for innate immunity, Trends Genet. 9 (1993) 178–183.
[5] K. Takeda, S. Akira, Toll-like receptors in innate immunity, Int. Immunol. 17 (2005) 1–14.
[6] J.A. Hoffmann, Innate immunity of insects, Curr. Opin. Immunol. 7 (1995) 4–10.
[7] M.D. Lavine, M.R. Strand, Insect hemocytes and their role in immunity, Insect Biochem. Mol. Biol. 32 (2002) 1295–1309.
[8] S. Natori, H. Shiraishi, S. Hori, A. Kobayashi, The roles of Sarcophaga defense molecules in immunity and metamorphosis, Dev. Comp. Immunol. 23 (1999) 317–328.

[9] L.A. Rollins-Smith, Metamorphosis and the amphibian immune system, Immunol. Rev. 166 (1998) 221–230.
[10] J.A. Hoffmann, The immune response of Drosophila, Nature 426 (2003) 33–38.
[11] N. Silverman, Flies kNOw how to signal, Dev. Cell 4 (2003) 5–6.
[12] N.J. Russell, Cold adaptation of microorganisms, Philos. Trans. R. Soc. Lond. B Biol. Sci. 326 (1990) 595–608. discussion 608-11.
[13] G.D. Inglis, A.M. Lawrence, F.M. Davis, Pathogens associated with southwestern corn borers and southern corn stalk borers (Lepidoptera: Crambidae), J. Econ. Entomol. 93 (2000) 1619–1626.
[14] H. Chino, L.I. Gilbert, Diglyceride release from insect fat body: a possible means of lipid transport, Science 143 (1964) 359–361.
[15] A.J. Nappi, M. Silvers, Cell surface changes associated with cellular immune reactions in Drosophila, Science 225 (1984) 1166–1168.
[16] J. Robalino, C.L. Browdy, S. Prior, A. Metz, P. Parnell, P. Gross, G. Warr, Induction of antiviral immunity by double-stranded RNA in a marine invertebrate, J. Virol. 78 (2004) 10442–10448.
[17] F. Wang, H. Yang, F. Gao, G. Liu, Effects of acute temperature or salinity stress on the immune response in sea cucumber, Apostichopus japonicus, Comp. Biochem. Physiol. A Mol. Integr. Physiol. 151 (2008) 491–498.
[18] H. Wago, Cellular recognition of foreign materials by Bombyx mori phagocytes: I. Immunocompetent cells, Dev. Comp. Immunol. 6 (1982) 591–599.
[19] M. Ramet, P. Manfruelli, A. Pearson, B. Mathey-Prevot, R.A. Ezekowitz, Functional genomic analysis of phagocytosis and identification of a Drosophila receptor for E. Coli, Nature 416 (2002) 644–648.
[20] J. Ao, E. Ling, X.Q. Yu, Drosophila C-type lectins enhance cellular encapsulation, Mol. Immunol. 44 (2007) 2541–2548.
[21] M.B. el-Mandarawy, Effects of insect diapause and parasitization of a braconid, Bracon brevicornis Wesm. On the haemolymph of its host Sesamia cretica led, J. Egypt Soc. Parasitol. 27 (1997) 805–815.
[22] J. Rodrigues, F.A. Brayner, L.C. Alves, R. Dixit, C. Barillas-Mury, Hemocyte differentiation mediates innate immune memory in Anopheles gambiae mosquitoes, Science 329 (2010) 1353–1355.
[23] J. Krzemien, L. Dubois, R. Makki, M. Meister, A. Vincent, M. Crozatier, Control of blood cell homeostasis in Drosophila larvae by the posterior signalling centre, Nature 446 (2007) 325–328.

Laboratory Investigation (2011) 91, 972–977

PATHOBIOLOGY IN FOCUS

Induced pluripotent stem cells as a next-generation biomedical interface

Katherine E Hankowski[1], Takashi Hamazaki[1], Akihiro Umezawa[2] and Naohiro Terada[1]

Recent advances in DNA sequencing technologies and subsequent progress in genome-wide association study (GWAS) are rapidly changing the landscape of human diseases. Our knowledge on disease–gene linkage has been exponentially growing, and soon we will obtain complete maps of SNPs and mutations linked to nearly all major disease conditions. These studies will undoubtedly lead us to a more comprehensive understanding of how multiple genetic modifications link to human pathobiology. But what comes next after we discover these genetic linkages? To truly understand the mechanisms of how polygenic modifications identified through GWAS lead to disease conditions, we need an experimental interface to study their pathobiological effects. In this study, induced pluripotent stem cells (iPSCs), retaining all the genetic information from patients, will likely serve as a powerful resource. Indeed, pioneering studies have demonstrated that disease-specific iPSCs are useful for understanding disease mechanisms. Moreover, iPSC-derived cells, when recapitulating some disease phenotypes *in vitro*, can be a fast track screening tool for drug discovery. Further, with GWAS information, iPSCs will become a valuable tool to predict drug efficacy and toxicity for individuals, thus promoting personalized medicine. In this review, we will discuss how patient-specific iPSCs will become a powerful biomedical interface in clinical translational research.

Laboratory Investigation (2011) **91,** 972–977; doi:10.1038/labinvest.2011.85; published online 9 May 2011

KEYWORDS: clinical translational research; disease modeling; drug discovery; induced pluripotent stem cell; personalized medicine

Induced pluripotent stem cells (iPSCs) are pluripotent stem cells artificially generated by transiently expressing a set of exogenous transcription factors in somatic cells (Table 1). As Takahashi and Yamanaka[1] originally reported the method for iPSC induction in 2006, the field has been rapidly expanding with great expectation and with some concern for their appropriate use. Essentially, the clinical implications of iPSCs are twofold; first, as a cellular resource for transplantation therapy, and second, as a system to model human diseases. Although the former direction is years away and unlikely to be an immediate concern for most experimental pathologists, the latter potential may be more relevant. We feel now is a good time to overview the present status of iPSC research for used in disease mechanism studies in this pathology-oriented journal, to discuss the potential value of iPSCs in future disease biology studies, and also to address the limitations and obstacles that need to be overcome. As many excellent reviews have been published to date (eg, see Kiskinis and Eggan,[2] Stadtfeld and Hochedlinger,[3] Saha and Jaenisch,[4] Marchetto *et al*,[5] and Yoshida and Yamanaka[6]), here we will try to avoid redundancy as much as possible and bring a newer perspective to iPSC use in modeling clinical diseases.

iPSCs TO MODEL CLINICAL DISEASES?

When the technology to generate human iPSCs first became available,[7,8] immediate attention was placed on their potential for use in cell-based transplantation. Using *in vitro* differentiation, iPSCs, like embryonic stem cells (ESCs), can provide an unlimited source of useful cell types for transplantation. The use of iPSCs in research has been largely welcomed by society because they lack the substantial ethical concern of cellular origin, which plagues ESCs. The fact that the cells are autologous for patients could be another advantage in transplantation. A major drawback of iPSCs for transplantation use is their carcinogenic potential, although recent progress in reprogramming technologies is overcoming the problem (see Table 1).

[1]Department of Pathology, Center for Cellular Reprogramming, University of Florida College of Medicine, Gainesville, FL, USA and [2]Department of Reproductive Biology and Pathology, National Research Institute for Child Health and Development, Tokyo, Japan
Correspondence: Dr N Terada, MD, PhD, Department of Pathology, Center for Cellular Reprogramming, University of Florida College of Medicine, PO Box 100275, Gainesville, FL 32610, USA.
E-mail: terada@pathology.ufl.edu

Received 14 February 2011; revised 21 March 2011; accepted 31 March 2011

Table 1 Basic background of induced pluripotent stem cells (iPSCs)

What exactly are iPSCs?—The iPSCs are a type of pluripotent stem cell; which means, they can be propagated on culture dishes almost indefinitely (prolonged self renewal capacity) and can differentiate into all three germ layer lineage cells (pluripotency). In contrast to embryonic stem cells (ESCs), a prototype of pluripotent stem cells described below, iPSCs are generated from somatic cells, such as fibroblasts and keratinocytes, by forced expression of exogenous transcription factors. The fact that they do not need any embryonic components, fertilized eggs or oocytes in generation is considered an advantage of iPSCs over ESCs.

How are they made?—Originally, iPSCs were generated by retroviral transduction of a set of transcription factors (Oct4, Sox2, Klf4 and/or c-Myc) into fibroblasts.[1] It has been demonstrated that iPSCs can be made from various cell types including gastric epithelial cells, blood mononuclear cells, hepatocytes etc (see review Kiskinis and Eggan,[2] Stadtfeld and Hochedlinger,[3] Saha and Jaenisch,[4] Marchetto *et al*,[5] and Yoshida and Yamanaka[6]). Although the original retroviral method is still widely used, particularly for disease mechanism studies, alternative methods to eliminate potential genetic alterations such as gene integration have been intensively studied with the aim of using the cells for clinical transplantation in the future. These new methods use non-integrating vectors,[18,19] RNA transfer,[20] peptide transfer,[21] small chemicals[22,23] and so on (see review Kiskinis and Eggan[2] for details).

Are they identical to ESCs?—ESCs are a prototype of pluripotent stem cells, which, in the case of humans, are generated from unused *in vitro* fertilized eggs.[24] As ESCs have been intensively characterized already, they are considered to be a gold standard for pluripotent stem cells.[25] Self-renewing potentials and *in vitro* differentiation potentials are essentially indistinguishable between ESCs and iPSCs in later passages. However, recent studies revealed that they are not necessarily identical.[26–28] In particular, earlier passage iPSCs retain some epigenetic memories of the origin: ie, iPSCs derived from blood, for instance, have a trace of epigenetic profile of blood cells.[26,28] These epigenetic memories are considered to be lost during passages and iPSCs become more similar to ESCs.[28]

How can they be used in transplantation?—As iPSCs will differentiate heterogeneously in nature, it is essential to guide differentiation into certain lineages or purify specific cell types after differentiation before using them as a source of cellular transplantation. There are many practical protocols available now to induce differentiation of ESCs or iPSCs and enrich useful cell types such as motor neurons, cardiomyocytes and β-cells.[29] Such protocols are being constantly improved. Recently it has also been demonstrated possible to generate a whole rat organ from iPSCs using interspecies blastocyst complementation with mice.[30] Making a transplantable human organ from self-iPSCs in xenogenic animals, such as pigs, is within the scope of iPSC scientists.

Do they cause cancers? — The iPSCs generated from the original retrovirus method (particularly the one using c-Myc) were shown to be a cause of cancer in experimental animals.[31] These problems have been largely overcome at least in mouse models by recent technological improvements as described above.[6] However, more intensive tests will be required before their use in clinical trials to monitor long-term effects. Establishment of a universal method for iPSC generation for transplantation in terms of safety, efficiency, accessibility, reproducibility etc is desired and is yet to come. Another issue to be resolved is potential teratoma formation by undifferentiated iPSCs (or ESCs). Removal of undifferentiated iPSCs, if there are any, is required before cellular transplantation.

Soon after human iPSC technology was introduced, however, researchers also began to realize an additional and possibly greater value for the cells as a system to model human diseases. iPSCs can be generated from skin biopsies or blood samples of patients, and can be differentiated *in vitro* into cell types that are not easily accessible in patients, such as neurons and cardiomyocytes. As iPSCs retain all the genomic information from the original patients, iPSCs could be used to study how genetic aberrancies in the patient manifest in target cells *in vitro*.

One reason for advancement of hematopoietic disease understanding from molecular studies is ease of accessibility of blood or bone marrow samples for *in vitro* studies. Successful development of molecular-targeted drugs, such as imatinib, for the treatment of chronic myeloid leukemia represent a triumphal example of a successful outcome of long-term molecular study. In contrast to the blood, other patient tissues such as brain and heart are not easily accessible, which has been a substantial disadvantage for pathobiology studies in neural and cardiac disorders. Such drawbacks could be partly overcome by iPSC technology.

Skeptics can argue, of course, against this rather simple and bold scheme.[4,5] First, the cells obtained from *in vitro* differentiation of iPSC may be very different from equivalent cell types seen in real organs and tissues. Second, the cells will not likely fully or even closely recapitulate *in vivo* disease conditions, which are a consequence of complex systems with multiple cell types, and are due to the long-term effects by gene mutations. This is particularly a concern for late onset diseases. However, even when we see a part of the disease phenotypes or molecular changes in iPSC-derived cells, the system will be beneficial for defining and understanding disease mechanisms.

PIONEERING STUDIES OF DISEASE-SPECIFIC iPSCs

Despite some existing concerns, many pioneering studies have been conducted, some of which indeed demonstrate advantages to using patient iPSCs to understanding disease mechanisms and/or to identify novel therapeutic approaches. Table 2 summarizes the literature in which disease-specific iPSCs were generated. It should be noted that some papers listed in the table were not designed for disease biology study but rather intended for use in cell-based transplantation therapies in the future.

The first phase of research focused on demonstrating that iPSCs can be successfully generated from patients, and initial studies of this type were published as early as 2008. In an inaugural paper, Park *et al*[9] showed that they were able to generate human iPSCs from patients with a variety of genetic disorders, and these cells showed a similar pluripotent differentiation capacity equivalent to control iPSCs derived from normal individuals. Meanwhile, Dimos *et al*[10] generated iPSCs from ALS patients and differentiated them into motor neurons, *in vitro*, to demonstrate the potential of iPSC technology to produce a large amount of a disease-relevant cell type for research.

The second phase was to prove the concept that disease-iPSC-derived cells can indeed recapitulate some disease-specific effects *in vitro*. The first paper of this kind was published in January 2009 by Ebert *et al.*[11] Here the authors generated iPSCs from patients with spinal muscular atrophy (SMA) who have mutations in the survival motor neuron 1 (*SMN1*) gene. Interestingly, deletion of *SMN1* is partially compensated by a redundant *SMN2* gene in human patients, which can also generate a full-length SMN protein but only at a lower level. Notably, other model animals such as worms, flies and mice lack the *SMN2* gene, indicating that a model system in humans is essential for fully understanding disease mechanisms. Further, as targeted *SMN2* gene activation is a potential mechanism for curing the disease, only a human cell system would be useful for the research. The study demonstrated that motor neurons derived from SMA–iPSCs harbor deficits in morphology, survival and synapsin staining, which represents SMA clinical pathology in part. In addition, the authors demonstrated that drugs, which were previously known to induce *SMN2*-derived SMN protein, indeed increased the level of SMN protein in SMA–iPSCs, implying the iPSC system would be useful for future drug discovery. Similar to the SMA study, recapitulation of neural disease phenotypes *in vitro* using the iPSC system has been nicely demonstrated with familial dysautonomia[12] and Rett syndrome.[13] Further, iPSCs have been generated from long QT syndrome patients,[14,15] where studies demonstrated prolonged action potentials in patient-iPSC-derived cardiomyocytes and their arrhythmogenicity, recapitulating the disease phenotype *in vitro*. Notably, all of the studies described above also demonstrated a reversal of the observed phenotypes by previously known drugs, indicating the system is compatible with drug discovery.

The third phase would be to prove that iPSC studies will indeed lead to novel insights for disease biology, and/or identification of novel therapeutic approaches. The study by Agarwal *et al*[16] regarding dyskeratosis congenita (DC) may be the first in this category. DC is a disorder of telomere maintenance in which DKC1 mutation leads to destabilization of telomerase RNA component (TERC). Of interest, reprogramming into a pluripotency status increased the level of TERC despite the presence of DKC1 mutation and restored the telomere length. The discovery further led the authors to study and identify previously unidentified mechanisms of TERC upregulation, which could lead to a new therapeutic approach in the future. In Freidreich's ataxia,[17] an extension of GAA/TTC nucleotide repeat was seen during iPSC generation and prolonged culture, which was partially prevented by knocking down of the *MSH2* gene. These data also provided some newer insights regarding the disease progression.

The fourth phase, which has not yet been achieved, will be to demonstrate that iPSC research indeed leads to disease prevention or cure by discovery of effective therapeutic approaches or drugs. This would be the time when the technology truly reaches Nobel Prize status.

WHERE WILL WE SEE THE TRUE VALUE OF iPSCs?

As discussed above, disease biology studies using iPSCs are on the way, and are progressing steadily with encouraging speed. Where will iPSCs likely show the most value in the near future? First, diseases that do not have high quality or appropriate animal models would benefit from iPSC study. In such cases, iPSC research has a great chance to facilitate disease understanding and/or drug discoveries. Indeed, we could say that iPSCs, which can be generated directly from patients relatively easily, are a fast track research tool when compared with other model systems in which we need to induce gene modifications (Figure 1). Moreover, iPSCs are a fast track research tool in clinical translational research for an additional reason. As a cellular system, disease iPSCs or iPSC-derived cells are directly applicable to drug screening. Importantly, we can achieve these schemes not only within relatively short time but also with relatively low cost when compared with the classical approaches in which we first identified the causes and then generated models to recapitulate them. These features may be particularly good news for research of rare diseases, which lack a large budget. In addition to the studies published (Table 2), a considerable number of research labs around the world are currently generating iPSCs from a variety of rare diseases. It may not be long until we hear promising discoveries of novel approaches or drugs to cure some of these diseases.

Since the first transgenic and knockout mouse studies were published in 1980 and 1989, respectively, mice have been extensively used to model human diseases. There is no doubt their contributions to medicine are and will be countless, and indeed the development of knockout mouse technology was awarded the 2007 Nobel Prize. However, we also know that

Table 2 Disease-specific-induced pluripotent stem cells (iPSCs), in studies published as of January 2011

Year of publications	Disease which human iPSCs are made from	References
2008	Amyotrophic lateral sclerosis	Dimos *et al*[10]
	ADA-SCID, Gaucher disease, Duchenne muscular dystrophy, Becker muscular dystrophy, Down syndrome, Parkinson's disease, juvenile diabetes mellitus, Swachman–Bodian–Diamond syndrome, Huntington's disease, Lesch–Nyhan syndrome	Park *et al*[9]
2009	Spinal muscular atrophy	Ebert *et al*[11]
	Parkinson's disease	Soldner *et al*[32]
	Rett syndrome	Hotta *et al*[33]
	Thalassemia, sickle cell anemia	Ye *et al*[34]
	Fanconi anemia	Raya *et al*[35]
	Type I diabetes	Maehr *et al*[36]
	Familial dysautonomia	Lee *et al*[12]
	Thalassemia	Wang *et al*[37]
	Myeloproliferative diseases	Ye *et al*[38]
2010	Duchenne muscular dystrophy	Kazuki *et al*[39]
	Dyskeratosis congenita	Agarwal *et al*[16]
	Fragile X syndrome	Urbach *et al*[40]
	Chronic myeloid leukemia	Carette *et al*[41]
	Leopard syndrome	Carvajal-Vergara *et al*[42]
	Liver diseases: α1-antitrypsin deficiency, familial hypercholesterolemia, glycogen storage disease type 1a, Crigler–Najjar, tyrosinemia type 1	Rashid *et al*[43]
	Parkinson's disease	Hargus *et al*[44]
	Lung diseases: cystic fibrosis, α-1 antitrypsin deficiency-related emphysema, scleroderma, and sickle-cell disease	Somers *et al*[45]
	Long QT syndrome	Moretti *et al*[15]
	Angelman syndrome, Prader–Willi syndrome	Chamberlain *et al*[46]
	Huntington's disease	Zhang *et al*[47]
	Friedreich's ataxia	Ku *et al*[17]
	Rett syndrome	Marchetto *et al*[13]
	Parkinson's disease	Cooper *et al*[48]
	Prader–Willi syndrome	Yang *et al*[49]
2011	Hutchinson Gilford progeria	Zhang *et al*[50]
	Hurler syndrome	Tolar *et al*[51]
	Recessive dystrophic epidermolysis bullosa	Tolar *et al*[52]
	Primary immunodeficiency	Pessach *et al*[53]
	Long QT syndrome	Itzhaki *et al*[14]

Note that some papers listed here were not designed for disease biology study but rather aimed for cell-based transplantation therapies. Although we tried to generate a comprehensive table of disease-specific human iPSCs published in peer-reviewed journals at the present moment, we may have missed some papers in the literature.

many human diseases are complex polygenic diseases, which are not easily recapitulated by gene modifications in mice. In the era of genome-wide association study (GWAS), when we accumulate our knowledge of polygenetic linkage to diseases, an alternative model to recapitulate the polygenic modifications is highly desired. In other words, in order to truly understand mechanisms of how polygenic modifications identified through GWAS lead to disease conditions, we need